was partially associated with SVR in a study of patients with HCV genotype 2 who were treated with PEG IFN-α-2b and ribavirin.[13,14,16,33,34] The clear suggestion of a correlation between the SNP of IL-28B with IFN responsiveness would not be supported in patients with low HCV RNA levels because of the high SVR rate and predominant genotype 2.

Viral factors associated with SVR have been studied, and several regions, including 5′-untranslated region, core, E2, NS5A and NS5B, have been suggested to play important roles in IFN responsiveness.[14,16,35–38] Further studies need to investigate whether these other viral factors, especially interferon and ribavirin resistance-determining region of NS5A and core amino acid substitutions, among patients with low HCV RNA levels affect the response to PEG IFN monotherapy.

Hepatitis C virus RNA levels could be easy to measure using commercial kits and would be useful for clinical practice, but sequencing analysis, which involves much effort and cost, would be needed to characterize the ISDR. SVR was achieved in 95.1% of patients with lower HCV RNA levels (<50 KIU/mL) and 98.4% of patients with mutant type. ISDR was a better factor, but HCV RNA level might be used as a predictive factor instead of measurement of ISDR.

The definition of the low HCV RNA level that was related to a good response to IFN therapy has varied widely, from 100–600 KIU/mL.[7,9–11] Zeuzem *et al.* reported that 24 weeks of therapy with PEG IFN-α-2b plus ribavirin is insufficient for the treatment of patients with HCV genotype 1 and a HCV RNA level of 600 KIU/mL or less.[10] They suggested that patients with HCV RNA of 250 KIU/mL or less would have a good response to PEG IFN-α-2b and ribavirin combination therapy for 24 weeks. Most reports from Japan defined 100 KIU/mL as the cut-off level for low HCV levels and used standard IFN monotherapy.[4,7,9,11] The outcome that would maximize the efficacy of IFN therapy would depend on the relationships between the cut-off HCV RNA level and therapeutic regimens. The optimal cut-off level for low HCV levels and the matching therapeutic regimens are not well understood, and further studies are needed to clarify these issues.

Based on the SVR in patients receiving therapy for 24 weeks compared to those treated for 48 weeks, there was no difference in IFN responsiveness by duration in this small study. However, this study was not a randomized study. Further studies are needed to investigate the optimal duration of PEG IFN-α-2a monotherapy for patients with low HCV RNA levels.

Pascu *et al.* performed a meta-analysis for the correlation between SVR and ISDR in patients with HCV genotype 1b infection who received standard IFN therapy.[19] They found that 11 of 21 European patients with mutant type ISDR and HCV RNA levels of less than 6.6 log copies/mL achieved SVR, but 67 of 69 Japanese patients with mutant type ISDR and HCV RNA levels of less than 6.6 log copies/mL achieved SVR. The mode of HCV infection and geographical and racial differences would have effects on the prediction of SVR by ISDR.[39,40] As a result, the ISDR system is more suitable for predicting SVR in Asian than in European patients. Although validation of these observations in larger cohorts is required, mutations in the ISDR were useful for predicting the response to PEG IFN-α-2a monotherapy in patients with low HCV levels.

In conclusion, in patients with HCV infection, low HCV levels and more than two mutations in the ISDR are significantly associated with a good response to PEG IFN-α-2a monotherapy. An individualized treatment strategy based on HCV RNA levels and the ISDR in patients with chronic hepatitis C would be useful in clinical practice.

REFERENCES

1 Seeff LB. Natural history of chronic hepatitis C. *Hepatology* 2002; **36**: S35–46.
2 Hoofnagle JH, Seeff LB. Peginterferon and ribavirin for chronic hepatitis C. *N Engl J Med* 2006; **355**: 2444–51.
3 Ghany MG, Strader DB, Thomas DL, Seeff LB, American Association for the Study of Liver Diseases. Diagnosis, management, and treatment of hepatitis C: an update. *Hepatology* 2009; **49**: 1335–74.
4 Kumada H, Okanoue T, Onji M *et al.* Guidelines for the treatment of chronic hepatitis and cirrhosis due to hepatitis C virus infection for the fiscal year 2008 in Japan. *Hepatol Res* 2010; **40**: 8–13.
5 McHutchison JG, Everson GT, Gordon SC *et al.* Telaprevir with peginterferon and ribavirin for chronic HCV genotype 1 infection. *N Engl J Med* 2009; **360**: 1827–38.
6 Kwo PY, Lawitz EJ, McCone J *et al.* Efficacy of boceprevir, an NS3 protease inhibitor, in combination with peginterferon alfa-2b and ribavirin in treatment-naive patients with genotype 1 hepatitis C infection (SPRINT-1): an open-label, randomised, multicentre phase 2 trial. *Lancet* 2010; **376**: 705–16.
7 Yokosuka O, Iwama S, Suzuki N *et al.* High sustained virologic response rate after interferon monotherapy in Japanese hepatitis C patients with a low HCV RNA titer and/or HCV genotype 2. A prospective study. *Intervirology* 2004; **47**: 328–34.

8 Tabaru A, Narita R, Hiura M, Abe S, Otsuki M. Efficacy of short-term interferon therapy for patients infected with hepatitis C virus genotype 2a. *Am J Gastroenterol* 2005; **100**: 862–7.
9 Kawamura Y, Arase Y, Ikeda K *et al.* The efficacy of short-term interferon-beta therapy for chronic hepatitis C patients with low virus load. *Intern Med* 2008; **47**: 355–60.
10 Zeuzem S, Buti M, Ferenci P *et al.* Efficacy of 24 weeks treatment with peginterferon alfa-2b plus ribavirin in patients with chronic hepatitis C infected with genotype 1 and low pretreatment viremia. *J Hepatol* 2006; **44**: 97–103.
11 Arase Y, Suzuki F, Akuta N *et al.* Combination therapy of peginterferon and ribavirin for chronic hepatitis C patients with genotype 1b and low-virus load. *Intern Med* 2009; **48**: 253–8.
12 Okanoue T, Itoh Y, Hashimoto H *et al.* Predictive values of amino acid sequences of the core and NS5A regions in antiviral therapy for hepatitis C: a Japanese multi-center study. *J Gastroenterol* 2009; **44**: 952–63.
13 Tanaka Y, Nishida N, Sugiyama M *et al.* Genome-wide association of IL28B with response to pegylated interferon-alpha and ribavirin therapy for chronic hepatitis C. *Nat Genet* 2009; **41**: 1105–9.
14 Akuta N, Suzuki F, Hirakawa M *et al.* Amino acid substitution in hepatitis C virus core region and genetic variation near the interleukin 28B gene predict viral response to telaprevir with peginterferon and ribavirin. *Hepatology* 2010; **52**: 421–9.
15 Hayashi K, Katano Y, Ishigami M *et al.* Mutations in the core and NS5A region of hepatitis C virus genotype 1b and correlation with response to pegylated-interferon-alpha 2b and ribavirin combination therapy. *J Viral Hepat* 2011; **18**: 280–6.
16 Hayashi K, Katano Y, Honda T *et al.* Association of interleukin 28B and mutations in the core and NS5A region of hepatitis C virus with response to peg-interferon and ribavirin therapy. *Liver Int* 2011; **31**: 1359–65.
17 Enomoto N, Sakuma I, Asahina Y *et al.* Mutations in the nonstructural protein 5A gene and response to interferon in patients with chronic hepatitis C virus 1b infection. *N Engl J Med* 1996; **334**: 77–81.
18 Nakano I, Fukuda Y, Katano Y, Nakano S, Kumada T, Hayakawa T. Why is the interferon sensitivity-determining region (ISDR) system useful in Japan? *J Hepatol* 1999; **30**: 1014–22.
19 Pascu M, Martus P, Höhne M *et al.* Sustained virological response in hepatitis C virus type 1b infected patients is predicted by the number of mutations within the NS5A-ISDR: a meta-analysis focused on geographical differences. *Gut* 2004; **53**: 1345–51.
20 Yen YH, Hung CH, Hu TH *et al.* Mutations in the interferon sensitivity-determining region (nonstructural 5A amino acid 2209-2248) in patients with hepatitis C-1b infection and correlating response to combined therapy of pegylated interferon and ribavirin. *Aliment Pharmacol Ther* 2008; **27**: 72–9.
21 Muñoz de Rueda P, Casado J, Patón R *et al.* Mutations in E2-PePHD, NS5A-PKRBD, NS5A-ISDR, and NS5A-V3 of hepatitis C virus genotype 1 and their relationships to pegylated interferon-ribavirin treatment responses. *J Virol* 2008; **82**: 6644–53.
22 Gale M Jr, Blakely CM, Kwieciszewski B *et al.* Control of PKR protein kinase by hepatitis C virus nonstructural 5A protein: molecular mechanisms of kinase regulation. *Mol Cell Biol* 1998; **18**: 5208–18.
23 Sáiz JC, López-Labrador FX, Ampurdanés S *et al.* The prognostic relevance of the nonstructural 5A gene interferon sensitivity determining region is different in infections with genotype 1b and 3a isolates of hepatitis C virus. *J Infect Dis* 1998; **177**: 839–47.
24 Murakami T, Enomoto N, Kurosaki M, Izumi N, Marumo F, Sato C. Mutations in nonstructural protein 5A gene and response to interferon in hepatitis C virus genotype 2 infection. *Hepatology* 1999; **30**: 1045–53.
25 Sarrazin C, Kornetzky I, Rüster B *et al.* Mutations within the E2 and NS5A protein in patients infected with hepatitis C virus type 3a and correlation with treatment response. *Hepatology* 2000; **31**: 1360–70.
26 Dal Pero F, Tang KH, Gerotto M *et al.* Impact of NS5A sequences of Hepatitis C virus genotype 1a on early viral kinetics during treatment with peginterferon- alpha 2a plus ribavirin. *J Infect Dis* 2007; **196**: 998–1005.
27 Nagase Y, Yotsuyanagi H, Okuse C *et al.* Effect of treatment with interferon alpha-2b and ribavirin in patients infected with genotype 2 hepatitis C virus. *Hepatol Res* 2008; **38**: 252–8.
28 Hayashi K, Katano Y, Honda T *et al.* Mutations in the interferon sensitivity-determining region of hepatitis C virus genotype 2a correlate with response to pegylated-interferon-alpha 2a monotherapy. *J Med Virol* 2009; **81**: 459–66.
29 Ge D, Fellay J, Thompson AJ *et al.* Genetic variation in IL28B predicts hepatitis C treatment-induced viral clearance. *Nature* 2009; **461**: 399–401.
30 Otagiri H, Fukuda Y, Nakano I *et al.* Evaluation of a new assay for hepatitis C virus genotyping and viral load determination in patients with chronic hepatitis C. *J Virol Methods* 2002; **103**: 137–43.
31 Hayashi K, Fukuda Y, Nakano I *et al.* Prevalence and characterization of hepatitis C virus genotype 4 in Japanese hepatitis C carriers. *Hepatol Res* 2003; **25**: 409–14.
32 Simmonds P, Bukh J, Combet C *et al.* Consensus proposals for a unified system of nomenclature of hepatitis C virus genotypes. *Hepatology* 2005; **42**: 962–73.
33 Mangia A, Thompson AJ, Santoro R *et al.* An IL28B polymorphism determines treatment response of hepatitis C virus genotype 2 or 3 patients who do not achieve a rapid virologic response. *Gastroenterology* 2010; **139**: 821–7.

34 Akuta N, Suzuki F, Seko Y *et al.* Association of IL28B genotype and viral response of hepatitis C virus genotype 2 to interferon plus ribavirin combination therapy. *J Med Virol* 2012; **84:** 1593–9.
35 Akuta N, Suzuki F, Sezaki H *et al.* Association of amino acid substitution pattern in core protein of hepatitis C virus genotype 1b high viral load and non-virological response to interferon-ribavirin combination therapy. *Intervirology* 2005; **48:** 372–80.
36 Watanabe K, Yoshioka K, Yano M *et al.* Mutations in the nonstructural region 5B of hepatitis C virus genotype 1b: their relation to viral load, response to interferon, and the nonstructural region 5A. *J Med Virol* 2005; **75:** 504–12.
37 Katano Y, Hayashi K, Ishigami M *et al.* Association with 5′-untranslated region and response to interferon in chronic hepatitis C. *Hepatogastroenterology* 2007; **54:** 854–7.
38 El-Shamy A, Nagano-Fujii M, Sasase N *et al.* Sequence variation in hepatitis C virus nonstructural protein 5A predicts clinical outcome of pegylated interferon/ribavirin combination therapy. *Hepatology* 2008; **48:** 38–47.
39 Layden-Almer JE, Kuiken C, Ribeiro RM *et al.* Hepatitis C virus genotype 1a NS5A pretreatment sequence variation and viral kinetics in African American and white patients. *J Infect Dis* 2005; **192:** 1078–87.
40 Jenke AC, Moser S, Orth V, Zilbauer M, Gerner P, Wirth S. Mutation frequency of NS5A in patients vertically infected with HCV genotype 1 predicts sustained virological response to peginterferon alfa-2b and ribavirin combination therapy. *J Viral Hepat* 2009; **16:** 853–9.

Hepatology Research

Hepatology Research 2013 doi: 10.1111/hepr.12049

Original Article

Utility of computed tomography fusion imaging for the evaluation of the ablative margin of radiofrequency ablation for hepatocellular carcinoma and the correlation to local tumor progression

Yuki Makino,[1] Yasuharu Imai,[1] Takumi Igura,[1] Masatoshi Hori,[3] Kazuto Fukuda,[1] Yoshiyuki Sawai,[1] Sachiyo Kogita,[1] Hideko Ohama,[1] Yasushi Matsumoto,[1] Masanori Nakahara,[1] Shinichiro Zushi,[1] Masanori Kurokawa,[1] Keisuke Isotani,[2] Manabu Takamura,[2] Norihiko Fujita[2] and Takamichi Murakami[4]

Departments of [1]Gastroenterology and [2]Radiology, Ikeda Municipal Hospital, Ikeda, [3]Department of Radiology, Osaka University Graduate School of Medicine, Suita, and [4]Department of Radiology, Kinki University School of Medicine, Osakasayama, Japan

Aim: To demonstrate the usefulness of the computed tomography (CT) fusion imaging for the evaluation of treatment effect of radiofrequency ablation (RFA) for hepatocellular carcinoma (HCC).

Methods: Eighty-five patients with 94 HCC with complete ablation judged on conventional side-by-side interpretation of pre-RFA and post-RFA CT at the time of RFA were included in this retrospective study. CT data was retrospectively used to create fusion images of pre-RFA and post-RFA CT using automatic rigid registration and manual correction referring to intrahepatic structures and hepatic contours around a tumor. Clinical factors including a minimal ablative margin (MAM) measured on fusion images were examined to prove risk factors for local tumor progression (LTP).

Results: LTP was observed in 13 (13.8%) tumors with a median follow up of 21.0 months (range, 2–75). The mean MAM on the fusion image was 1.4 ± 3.1 mm and 23 tumors (24.5%) were judged to be protruding from the ablation zone. Multivariate analysis revealed that protruding from the ablation zone was the only significant factor for LTP (hazard ratio, 7.09; 95% confidential interval, 2.26–22.3; $P < 0.001$).

Conclusion: Some HCC were assessed as incomplete ablation on the CT fusion images, although considered completely ablated on side-by-side images at the time of treatment, and incomplete ablation was revealed to be the only independent risk factor for LTP. The CT fusion imaging enables quantitative and accurate evaluation of treatment effect of RFA.

Key words: ablative margin, computed tomography fusion imaging, hepatocellular carcinoma, local tumor progression, radiofrequency ablation

INTRODUCTION

HEPATOCELLULAR CARCINOMA (HCC) is one of the most common malignant neoplasms developed from chronic liver diseases.[1] In Japan HCC is ranked third and fifth among males and females, respectively, as a cause of death from malignant neoplasms.[2] The treatments for HCC such as surgical resection, liver transplant, percutaneous locoregional treatment, transcatheter arterial chemoembolization (TACE) and molecular targeted agents are chosen depending on staging and hepatic functional reserve, as well as general conditions.[3–5]

Percutaneous locoregional treatment is usually indicated for HCC up to three nodules and 3 cm in diameter.[3–5] Although percutaneous ethanol injection therapy (PEIT) used to play the central role for locoregional treatment in Japan, radiofrequency ablation (RFA), which was introduced in 1999, is now mainly used because RFA is considered superior to PEIT in terms of both recurrence and survival rate.[6]

In RFA, an electrode is inserted into a tumor under real-time guidance of ultrasonography (US) or

Correspondence: Dr Yasuharu Imai, Department of Gastroenterology, Ikeda Municipal Hospital, 3-1-18, Johnan, Ikeda, Osaka 563-8510, Japan. Email: yasuimai@hosp.ikeda.osaka.jp
Received 15 July 2012; revision 9 December 2012; accepted 16 December 2012.

laparoscopy, then the tumor and normal liver parenchyma surrounding the electrode is destroyed by heating via radiofrequency electric current.[7,8] Because an ablated tumor becomes obscure on US during treatment because of surrounding high echoic bubbles, the therapeutic effect of RFA is usually evaluated using dynamic CT performed a few days after RFA.

However, it is quite difficult to grasp the positional relation of the tumor and ablation zone visually and measure the ablative margin accurately, because pre-RFA and post-RFA CT are usually compared side-by-side. In this study, we created a fusion image of the pre-RFA and post-RFA CT, with a retrospective use of CT data, and tried overlaying a tumor on the ablation zone to comprehend their locational relation easily, which enables us to measure the minimal ablative margin (MAM) quantitatively. Then, we examined significant risk factors for local tumor progression (LTP) retrospectively, analyzing clinical factors including the MAM measured on the CT fusion image.

METHODS

Patients and tumors

THIS RETROSPECTIVE STUDY was approved by our institutional review board and informed consent of this study was waived. From January 2006 to September 2011, a total of 546 patients with 738 HCC nodules underwent RFA in our hospital. Of these nodules, 644 nodules were excluded for the following reasons: LTP lesions after previous treatment ($n = 35$), treatment of TACE or transarterial infusion before RFA ($n = 488$), lack of pre-RFA dynamic CT or CT angiography taken within 1 month before RFA ($n = 32$), no apparent tumor images on pre-RFA CT ($n = 66$), lack of post-RFA dynamic CT taken within 7 days after RFA ($n = 15$), followed up for less than 6 months after RFA ($n = 5$) and no additional RFA in spite of an obvious residual lesion ($n = 3$). The remaining 85 patients with 94 nodules were included in this study.

The diagnosis of hypervascular HCC was based on the typical imaging features at dynamic CT, CT angiography or gadolinium-ethoxybenzyl-diethylenetriamine pentaacetic acid (Gd-EOB-DTPA)-enhanced multiple resonance imaging (MRI).[9] The diagnosis of hypovascular HCC was made by US-guided biopsy.[10,11]

RFA procedure

Radiofrequency ablation was performed by one of three operators with more than 10 years of experience. All tumors were treated percutaneously under real-time US guidance. If the nodule was located on the liver surface, in the hepatic dome or adjacent to the gastrointestinal tract or gallbladder, we used artificial pleural effusion or ascites with 250–1500 mL of 5% glucose solution.

After 1% lidocaine was injected at the puncture site as local anesthesia, a 17-G cool-tip single electrode with a 2 or 3 cm exposed tip (Cool-tip RF Ablation System; Covidien, Boulder, CO, USA) was introduced under conscious sedation using 0.025–0.5 mg fentanyl citrate. After insertion of the electrode, ablation was started with an initial power output of 20 W or 30 W for the 2 cm or 3 cm active tip of the electrode, respectively, which was increased at a rate of 10 W/min until roll-off. After roll-off, the output was set at the energy level just before roll-off and maintained until the fifth roll-off occurred or 12 min had passed since the start of ablation. After tumor ablation was completed, the electrode was pulled back ablating the needle track at 40 W output.

Follow up

Follow-up dynamic CT was performed within 7 days after RFA to evaluate treatment effect. The median interval between pre-RFA CT and post RFA CT was 27 days with a range of 14–38 days. All images were assessed side-by-side by the consensus of one radiologist with more than 10 years of experience and the operator of RFA. We defined complete ablation as meeting both of the following conditions: (i) no portion of tumor stain was present around the coagulated area in the arterial phase; and (ii) the coagulated area circumferentially extended beyond an estimated tumor boundary in the portal and equilibrium phases. If residual tumor was suspected, we repeated RFA until these conditions had been satisfied.

After complete ablation was attained, follow-up dynamic CT or Gd-EOB-DTPA-enhanced MRI and blood tests were performed every 3 months. If recurrence was suspected, additional imaging studies such as Gd-EOB-DTPA-enhanced MRI, dynamic CT and CT angiography were performed to confirm the diagnosis if necessary. LTP was defined as development of new tumor enhancement in contact with the ablation zone for both hypovascular and hypervascular HCC.

CT and MRI acquisition

Dynamic CT and CT angiography were performed by either 8-channel multidetector row helical CT (MDCT) (LightSpeed Ultra; GE Healthcare Japan, Tokyo, Japan) or 64-channel MDCT (Discovery CT 750HD; GE

Healthcare Japan). The slice thickness was 1.25 mm ($n = 19$) or 5.0 mm ($n = 75$). The pixel size on the X-Y plane was 0.68 mm in all cases. In the dynamic CT, 2.0 mL/kg of non-ionic contrast material with a concentration of 300 mgI/mL was i.v. injected with a fixed duration of 30 s using an automatic injector. Images were obtained at approximately 35–45, 65–80 and 190–205 s after the initiation of the contrast material injection for the arterial, portal and equilibrium phases, respectively.[9]

For CT angiography, two catheters inserted through the right or left femoral artery by the Seldinger technique were selectively placed, one in the superior mesenteric artery for CT during arterioportography (CTAP) and the other in the common hepatic artery for CT during hepatic arteriography (CTHA). CTAP images were obtained 30–33 s after injection of 66–80 mL of 150–160 mgI/mL non-ionic contrast medium at a rate of 2.0 mL/s. CTHA images were obtained 5–8 s after administration of 20–33 mL of 150–160 mgI/mL non-ionic contrast material at a rate of 1.0 mL/s.[12]

Gadolinium-ethoxybenzyl-diethylenetriamine pentaacetic acid-enhanced MRI was performed with a 1.5-T system (Signa Excite HD 1.5T; GE Healthcare Japan). The slice thickness was 5.0 mm. At first, an unenhanced MRI was obtained using a T_1-weighted gradient echo sequence (dual echoes; in-phase and out-of-phase). Then, unenhanced, arterial, portal, late and hepatobiliary phase images were acquired just before, 25 s, 70 s, 180 s and 20 min, respectively, after bolus injection of 25 μM/kg bodyweight (0.1 mL/kg) Gd-EOB-DTPA at a rate of 2.0 mL/s.[9,11]

CT fusion image creation

Fusion images were created by one radiologist with more than 10 years of experience who was blind to the information of LTP.

All CT images were sent to a workstation (Advantage Workstation Volumeshare 4; GE Healthcare Japan) equipped with the necessary software (Integrated Registration; GE Healthcare Japan) and the fusion images of pre-RFA CT (dynamic CT or CT angiography performed within 1 month before RFA) and post-RFA CT (arterial or portal phase of dynamic CT performed within 7 days after RFA) were created. As pre-RFA CT images for the CT fusion image creation, the phase in which the tumor size was the largest was chosen.

At first, pre-RFA and post-RFA images were fused by automatic image registration using a rigid registration method, in which the distribution of CT values in the whole abdomen became similar between these two image sets based on positional data and landmarks such as vertebrae and contours of internal organs, without deformation. Then, in order to improve image similarity, especially around a tumor, manual correction was carried out with six parameters (translation and rotation in axial, coronal and sagittal planes), referring to intrahepatic structures such as blood vessels, cysts, scars or iodized oil of past treatment, and hepatic contours near the tumor (Fig. 1a–c).

After registration, one arbitrary landmark near the tumor was marked both on the pre-RFA and post-RFA CT and the registration error was measured (Fig. 1d). We considered up to 3.0 mm error to be within the permissible range. If the error exceeded 3.0 mm, the registration was repeated until the error came within 3.0 mm.

Evaluation of MAM

Pre-RFA and post-RFA CT images were evaluated side-by-side by a hepatologist and radiologist with consensus who had more than 10 years of experience and were blind to clinical information including the MAM on fusion images and LTP, as to whether all of them were completely ablated without residue.

Fusion images were interpreted by consensus by another hepatologist and radiologist with more than 10 years of experience, both of whom were different from the blind readers of side-by-side interpretation described above and blind to the information of LTP. The readers measured a MAM, which is the shortest distance between the boundaries of a tumor and the ablation zone on axial images. If a tumor was entirely included in the ablation zone, the measured value was defined as positive, whereas it was defined as negative if a tumor was protruding from the ablation zone.

Statistical analysis

Univariate analysis and multivariate analysis were performed to analyze data. For univariate analysis, we categorized all tumors into two groups according to each variable which could potentially be related to LTP: (i) age (<70 years or ≥70 years); (ii) sex (male or female); (iii) etiology (hepatitis C virus or not); (iv) α-fetoprotein (AFP) (<20 ng/mL or ≥20 ng/mL); (v) protein induced by vitamin K absence/antagonist-II (PIVKA-II) (<40 mAU/mL or ≥40 mAU/mL); (vi) Child–Pugh grade (A or B); (vii) number of tumors at the time of RFA (1 or ≥2); (viii) number of RFA sessions (1 or ≥2), (ix) tumor diameter (<15 mm or ≥15 mm); (x) past treatment history of HCC (yes or no); (xi) tumor vascularity (hypervascular or hypovascular); (xii)

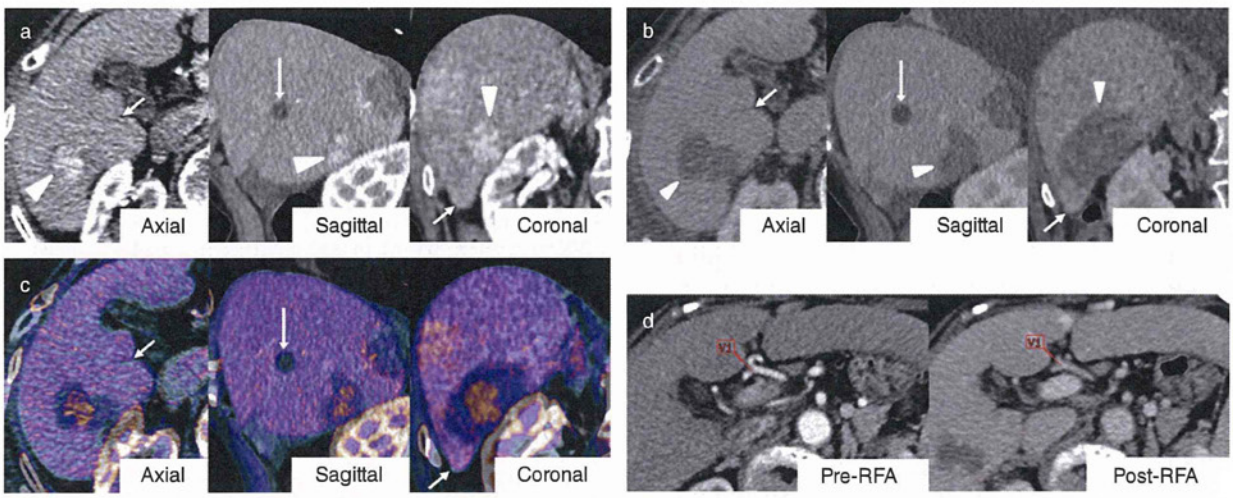

Figure 1 Creation of fusion images of pre-radiofrequency ablation (RFA) and post-RFA computed tomography (CT). (a) Hypervascular hepatocellular carcinoma (HCC) in segment 6 (arrowhead) was recognized on pre-RFA dynamic CT (arterial phase). (b) Ablation zone (arrowhead) was hypoattenuated on post-RFA dynamic CT (portal phase). (c) After automatic rigid registration, manual adjustment was added referring to intrahepatic structures such as cyst (long arrow) and hepatic contours (short arrow) around the tumor using six parameters (translation and rotation in axial, sagittal and coronal planes). For better discrimination of pre-RFA and post-RFA CT image, they were shown in color scale and gray scale, respectively. (d) After registration, one arbitrary landmark near the tumor was marked both on the pre-RFA and post-RFA CT and the registration error was measured. The registration error of this case was 1.48 mm. The slice thickness of both pre-RFA and post-RFA CT was 1.25 mm in this case.

presence of contiguous blood vessels (yes or no); (xiii) located in the hepatic dome (defined as within 5.0 mm beneath the diaphragm) (yes or no); (xiv) MAM (protruding from the ablation zone [a MAM of <0 mm] or not). The cumulative LTP rates of these two groups for each factor were estimated by the Kaplan–Meier method and the statistical significance was assessed using the log-rank test. Then, multivariate analysis using the stepwise Cox proportional hazard model was performed for the variables with $P < 0.20$ in univariate analysis to investigate independent risk factors for LTP.

The data were analyzed using SPSS ver. 11.0 software (SPSS, Chicago, IL, USA) and $P < 0.05$ was considered statistically significant.

RESULTS

Clinical characteristics and overall LTP

ALL 85 PATIENTS with 94 tumors were treated without treatment-related deaths and severe complications. Clinical characteristics are presented in Table 1. LTP was observed in 13 tumors (13.8%) with a median follow up of 21.0 months (range, 2–75) after RFA. The overall cumulative LTP rate at 1, 2 and 3 years

Table 1 Baseline characteristics of 85 patients with 94 tumors

Characteristics	Value
Age (years)†	71.8 ± 7.8
Sex (male/female)	62/23
Follow-up period (months)‡	21.0 (2–75)
Etiology (HBV/HCV/alcohol/others)	8/68/8/1
AFP (ng/mL)†	30.0 ± 62.9
PIVKA-II (mAU/mL)†	194 ± 1356
Child–Pugh grade (A/B)	63/22
No. of tumors at the time of RFA per patient†	1.5 ± 0.79
No. of RFA session per tumor†	1.3 ± 0.55
Tumor diameter (mm)†	14.0 ± 5.2
Past treatment history of HCC (yes/no)	61/24
Tumor vascularity (hypervascular/hypovascular)	75/19
Differentiation of hypovascular HCC (well/moderate)	18/1
No. of tumors with contiguous blood vessels	21
No. of tumors located in the hepatic dome	23
MAM per tumor (mm)†	1.4 ± 3.1

†Mean ± standard deviation (standard deviation).
‡Median.
AFP, α-fetoprotein; HBV, hepatitis B virus; HCC, hepatocellular carcinoma; HCV, hepatitis C virus; MAM, minimal ablative margin; PIVKA-II, protein induced by vitamin K absence/antagonist-II; RFA, radiofrequency ablation.

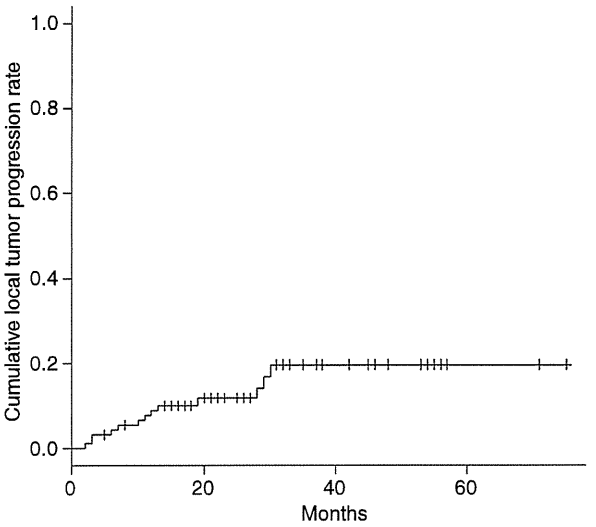

Figure 2 Cumulative local tumor progression rate in all tumors.

was 8.8%, 11.7% and 19.6%, respectively (Fig. 2). The mean time to LTP was 13.3 ± 9.7 months.

Fusion image creation and MAM

For the CT fusion image creation, the arterial phase ($n = 56$), portal phase ($n = 2$) or equilibrium phase ($n = 33$) of dynamic CT, CTHA ($n = 1$) or CTAP ($n = 2$) was used for the pre-RFA CT imaging and the arterial phase ($n = 52$) or portal phase ($n = 42$) were used for the post-RFA CT imaging. The minimal interval between conventional side-by-side assessment after RFA and the CT fusion creation was 8 months. In all 94 tumors, the CT fusion image could be created with a registration error of less than 3.0 mm and the mean error was 1.5 ± 0.68 mm. Total time required to create the fusion image was less than 15 min in all cases.

The mean MAM on the fusion image was 1.4 ± 3.1 mm (median, 1.8 mm; 25%–75% percentile, 0.0–3.3 mm). Twenty-three of the 94 tumors (24.5%) were judged to be protruding from the ablation zone by the CT fusion images, whereas five of the 94 tumors (5.3%) were considered to be protruding from the ablation zone by the consensus interpretation of side-by-side CT images by two blind readers.

Risk factors analysis of LTP

In univariate analysis, the potential factors for LTP with a *P*-value of less than 0.20 were designated as Child–Pugh grade B ($P = 0.037$), located in the hepatic dome ($P = 0.052$), and protruding from the ablation zone ($P < 0.001$) (Table 2). Multivariate analysis revealed that the only independent risk factor for LTP was protruding from the ablation zone (hazard ratio [HR], 7.09; 95% confidential interval [CI], 2.26–22.3; $P < 0.001$) (Table 3).

Table 2 Univariate analysis of possible risk factors for local tumor progression

Variables	*n*	*P*-value
Age (<70 years/≥70 years)	29/65	0.52†
Sex (male/female)	68/26	0.35†
Etiology (HCV or not)	77/17	0.78†
AFP (<20 ng/mL or ≥20 ng/mL)	60/34	0.34†
PIVKA-II (<40 mAU/mL or ≥40 mAU/mL)	70/24	0.28†
Child–Pugh grade (A/B)	68/26	0.037†
No. of tumors at the time of RFA (1/≥2)	56/38	0.87†
No. of RFA session (1/≥2)	73/21	0.41†
Tumor diameter (<15 mm/≥15 mm)	61/33	0.34†
Past treatment history of HCC (yes/no)	70/24	0.35†
Tumor vascularity (hypervascular/hypovascular)	75/19	0.38†
Presence of contiguous blood vessels (yes/no)	21/73	0.45†
Located in the hepatic dome (yes/no)	23/71	0.052†
Protruding from the ablation zone (yes/no)	23/71	<0.001†

†Log–rank test.
AFP, α-fetoprotein; HCC, hepatocellular carcinoma; HCV, hepatitis C virus; PIVKA-II, protein induced by vitamin K absence/antagonist-II; RFA, radiofrequency ablation.

Table 3 Multivariate analysis of risk factors for local tumor progression

Variables	HR	95% CI	*P*-value
Child–Pugh grade			
A	1.00		
B	3.12	0.96–10.1	0.058†
Located in the hepatic dome			
No	1.00		
Yes	2.67	0.87–8.24	0.087†
Protruding from the ablation zone			
No	1.00		
Yes	7.09	2.26–22.3	<0.001†

†Stepwise Cox proportional hazard model.
CI, confidential interval; HR, hazard ratio.

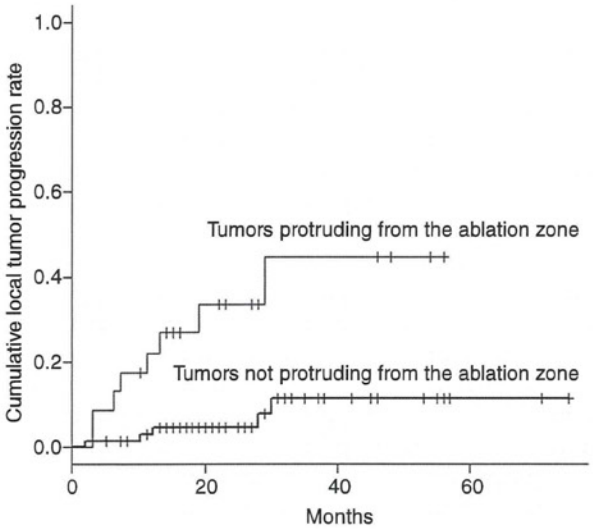

Figure 3 Cumulative local tumor progression rates in tumors that protrude from and do not protrude from the ablation zone. The tumors protruding from the ablation zone had significantly higher rates of cumulative local tumor progression ($P < 0.001$).

Relationship between MAM and LTP

The cumulative LTP rate at 1, 2 and 3 years was 22.0%, 33.5% and 44.6% in tumors protruding from the ablation zone and 4.5%, 4.5% and 11.4% in tumors not protruding from the ablation zone, respectively (Fig. 3). The cumulative LTP rate of tumors protruding from the ablation zone was significantly higher ($P < 0.001$).

Subsequently, all tumors were categorized into three groups on the basis of the MAM: group I (protruding from the ablation zone); group II (≥0 mm and <5.0 mm); and group III (≥5.0 mm) (Fig. 4). The cumulative LTP rate at 1, 2 and 3 years was 22.0%, 33.5% and 44.6% in group I ($n = 23$), 5.3%, 5.3% and 13.1% in group II ($n = 61$), and 0.0%, 0.0% and 0.0% in group III ($n = 10$), respectively. The log–rank test revealed statistical significance in the overall trend ($P = 0.002$), group I versus group II ($P = 0.002$) and group I versus group III ($P = 0.040$) (Fig. 5). Consequently, the cumulative LTP rate of group I was significantly higher than those of the other groups. Although significant difference was not observed between groups II and III, LTP was not observed in group III.

Among the 13 tumors resulting in LTP, LTP occurred at the same aspect of MAM on CT fusion images in 10 tumors (76.9%).

DISCUSSION

VARIOUS FACTORS RELATED to LTP after RFA have been reported so far, such as tumor diameter,[13–15] MAM,[16–19] PIVKA-II,[6] AFP[20] and location relative to the liver surface.[21] Although the MAM seems to be an important factor, only a few studies have examined the relationship between the MAM and LTP.[16–19,22]

In some studies, the MAM was estimated by comparing the pre-RFA and post-RFA CT in a side-by-side

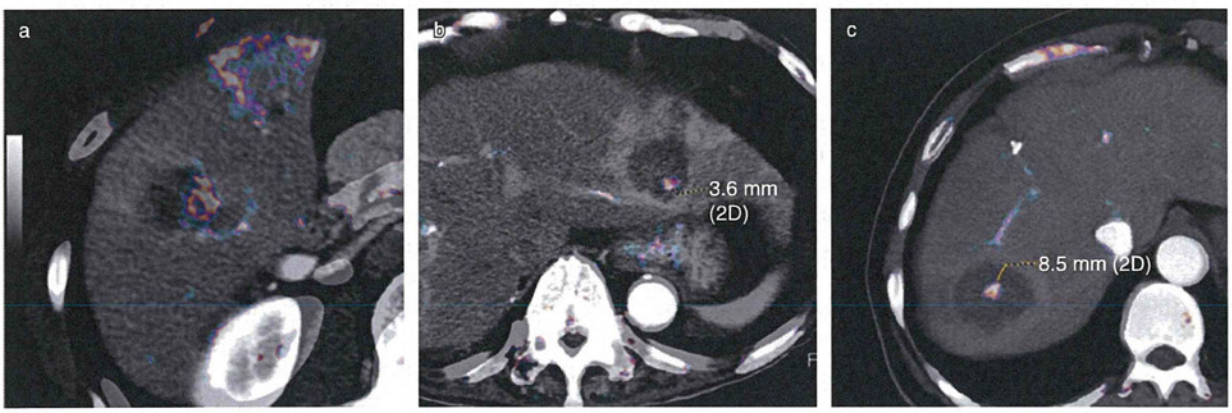

Figure 4 Categorization of tumors into three groups according to the value of the minimal ablative margin. (a) Group I, protruding from the ablation zone; (b) group II, larger than or equal to 0 mm and less than 5.0 mm; (c) group III, larger than or equal to 5.0 mm. Pre-radiofrequency ablation (RFA) and post-RFA computed tomography images were shown in color scale and gray scale, respectively, in order to clarify the locational relationship between the tumor and the boundary of the ablation zone.

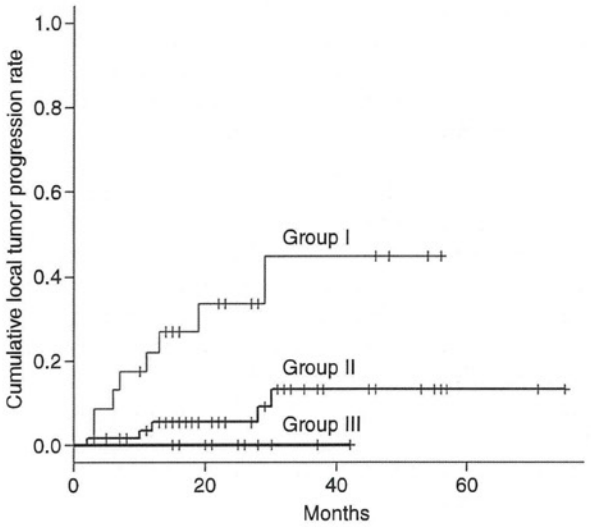

Figure 5 Cumulative local tumor progression rates according to the classification based on the minimal ablative margin. The cumulative local tumor progression rates were significantly different as a whole ($P = 0.002$), group I versus group II ($P = 0.002$), and group I versus group III ($P = 0.040$). Local tumor progression was not observed in group III.

manner.[17–19,22] However, it is possible that the evaluation tends to be somewhat subjective. In another study, the MAM was categorized into four groups on the basis of positional relation of iodized oil infused prior to RFA and the ablation zone.[16] Although the MAM can be evaluated objectively in this method, iodized oil may not be necessarily accumulated in a whole tumor.

Several studies on CT fusion images for the assessment of curative effect of RFA have been previously reported, which enables the objective evaluation of locational relation of the tumor and ablation zone.[23–27] However, this is the first study which investigated risk factors for LTP analyzing various clinical factors such as patient and tumor characteristics and laboratory data, in addition to the MAM measured on the CT fusion image. In this study, we have clearly shown that protruding from the ablation zone on the CT fusion image was the only independent factor for LTP. Above all, it deserves special consideration that as many as 23 tumors (24.5%) were regarded as protruding from the ablation zone on the fusion image, although all of them had been considered completely ablated at the time of treatment. Side-by-side interpretation at the time of treatment might have been affected by the operators' subjectivity. Nevertheless, all but five tumors (5.3%) were considered completely ablated by the blind interpretation of side-by-side CT images in this study. Thus, in evaluating the pre-RFA and post-RFA CT in a side-by-side manner, which is a standard practice at present, we may overlook tumors of incomplete ablation. On the contrary, fusion imaging technology enables us to grasp the positional relation objectively, resulting in more strict and accurate judgments.

A MAM of larger than or equal to 5.0 mm has been reported to be desirable[16,18] because of the presence of microsatellite lesions around a main tumor.[28] Therefore, we categorized all tumors into three groups on the basis of the MAM (Figs 4,5). As a result, although no significant difference was observed between groups II and III, the cumulative LTP rate differed depending on the value of a MAM. In particular, LTP did not occur in group III, although the number of tumors in group III was only 10 (10.6%). Kim *et al.* similarly reported that only 2.7% of cases could achieve a MAM of larger than or equal to 5.0 mm on fusion image, in contrast to 34.5% in a side-by-side interpretation.[26] Therefore, it may actually be quite difficult to attain a MAM of larger than or equal to 5.0 mm. However, a MAM of larger than or equal to 5.0 mm judged on fusion image may greatly lower the incidence of LTP.

Although it seems likely that all tumors protruding from the ablation zone eventually resulted in LTP because of residual tumor, LTP was observed in only eight tumors (34.8%). This result could be explained as follows. First, LTP might not have occurred yet during the observation period in some tumors protruding from the ablation zone. Second, some tumors might have been judged to be protruding from the ablation zone in error even if they had been completely ablated. This is partly because of the registration error of the fusion image. Because the permissive registration error was set at 3.0 mm in this study, measurement error might have occurred within this range. Moreover, limitations exist in the assessment of ablation zone using CT itself. Despite the locoregional registration just around the tumor, regional thermal deformity can take place after RFA. In addition, the heterogeneity at boundaries of the ablated regions on CT can be confusing for the assessment of the MAM. Subsequently, classification error of the MAM may happen in some cases.

For the fusion image creation, we adopted a rigid registration method in which the liver is regarded as a rigid body. The mean registration error around the tumor was 1.5 ± 0.68 mm and the fusion image could be created within 15 min in all cases in this study,

which seems clinically acceptable. Although a non-rigid registration method may be desirable for the registration of the whole liver taking account of deformation due to respiration and posture,[29] locoregional rigid registration around the tumor seems sufficient for the evaluation of treatment effect of RFA. Moreover, non-rigid registration may have some limitations. Tumors as well as ablation zones may be deformed in the process of registration. In addition, non-rigid registration may not be applied for cases with artificial ascites.[27] Therefore, comparative studies of rigid and non-rigid registration for the evaluation of treatment effect of RFA seem to be needed.

This study has some limitations. First, two types of slice thickness of CT images were used. Owing to the slice thickness, the measurement errors of, at most, 1.25 mm or 5.0 mm can occur on CT images with slice thicknesses of 1.25 mm or 5.0 mm, respectively. Moreover, on CT images with slice thickness of 5.0 mm, the spatial resolutions of reconstructed sagittal and coronal images were too low to evaluate the MAM accurately. Because the slice thicknesses of CT images used to create the fusion images were 5.0 mm in most cases, we evaluated the MAM on only the axial plane in all cases. Hence, the evaluation of the cranial and caudal side of a tumor may be somewhat inaccurate. In addition, due to the partial volume effect, the boundaries of tumor and ablation zone could be more obscure on CT images with the slice thickness of 5.0 mm. These points could have influenced the precision of the MAM, although pixel size on X-Y plane was uniform regardless of the slice thickness. Second, 19 HCC (20.2%) in our study were hypovascular. Because it seems quite difficult to distinguish residual tumor of hypovascular HCC or hypovascular recurrence from the adjacent low attenuated area of the ablation zone on dynamic CT, only hypervascular lesions were regarded as local recurrence in this study. Third, the number of tumors in this study is relatively small. Especially, the number of tumors in group III was so small that cumulative LTP rate was not significantly different between groups II and III. Further studies with a larger number of cases are needed to validate the value of 5.0 mm as a safety ablative margin.

In conclusion, the MAM measured on the CT fusion image was found to be significantly related to LTP. Above all, the CT fusion image could detect more tumors of incomplete ablation than side-by-side interpretation and these tumors actually showed higher LTP rates. CT fusion images enabled more quantitative and accurate evaluation of the curative effects of RFA than side-by-side assessment.

REFERENCES

1 Jemal A, Siegel R, Xu J, Ward E. Cancer statistics, 2010. *CA Cancer J Clin* 2010; **60**: 277–300.
2 Umemura T, Ichijo T, Yoshizawa K, Tanaka E, Kiyosawa K. Epidemiology of hepatocellular carcinoma in Japan. *J Gastroenterol* 2009; **44** (Suppl 19): 102–7.
3 Kudo M, Izumi N, Kokudo N *et al.* Management of hepatocellular carcinoma in Japan: Consensus-Based Clinical Practice Guidelines proposed by the Japan Society of Hepatology (JSH) 2010 updated version. *Dig Dis* 2011; **29**: 339–64.
4 European Association for the Study of the Liver; European Organisation For Research And Treatment Of Cancer. EASL-EORTC clinical practice guidelines: management of hepatocellular carcinoma. *J Hepatol* 2012; **56**: 908–43.
5 Bruix J, Sherman M, American Association for the Study of Liver Diseases. Management of hepatocellular carcinoma: an update. *Hepatology* 2011; **53**: 1020–2.
6 Shiina S, Tateishi R, Arano T *et al.* Radiofrequency ablation for hepatocellular carcinoma: 10-year outcome and prognostic factors. *Am J Gastroenterol* 2012; **107**: 569–77.
7 Haemmerich D. Biophysics of radiofrequency ablation. *Crit Rev Biomed Eng* 2010; **38**: 53–63.
8 Haemmerich D, Laeseke PF. Thermal tumour ablation: devices, clinical applications and future directions. *Int J Hyperthermia* 2005; **21**: 755–60.
9 Onishi H, Kim T, Imai Y *et al.* Hypervascular hepatocellular carcinomas: detection with gadoxetate disodium-enhanced MR imaging and multiphasic multidetector CT. *Eur Radiol* 2012; **22**: 845–54.
10 International Consensus Group for Hepatocellular Neoplasia. Pathologic diagnosis of early hepatocellular carcinoma: a report of the international consensus group for hepatocellular neoplasia. *Hepatology* 2009; **49**: 658–64.
11 Kogita S, Imai Y, Okada M *et al.* Gd-EOB-DTPA-enhanced magnetic resonance images of hepatocellular carcinoma: correlation with histological grading and portal blood flow. *Eur Radiol* 2010; **20**: 2405–13.
12 Imai Y, Murakami T, Yoshida S *et al.* Superparamagnetic iron oxide-enhanced magnetic resonance images of hepatocellular carcinoma: correlation with histological grading. *Hepatology* 2000; **32**: 205–12.
13 Komorizono Y, Oketani M, Sako K *et al.* Risk factors for local recurrence of small hepatocellular carcinoma tumors after a single session, single application of percutaneous radiofrequency ablation. *Cancer* 2003; **97**: 1253–62.
14 Lam VW, Ng KK, Chok KS *et al.* Risk factors and prognostic factors of local recurrence after radiofrequency ablation of hepatocellular carcinoma. *J Am Coll Surg* 2008; **207**: 20–9.
15 Lam VW, Ng KK, Chok KS *et al.* Incomplete ablation after radiofrequency ablation of hepatocellular carcinoma: analysis of risk factors and prognostic factors. *Ann Surg Oncol* 2008; **15**: 782–90.

16 Nishikawa H, Inuzuka T, Takeda H *et al.* Percutaneous radiofrequency ablation therapy for hepatocellular carcinoma: a proposed new grading system for the ablative margin and prediction of local tumor progression and its validation. *J Gastroenterol* 2011; **46**: 1418–26.
17 Liu CH, Arellano RS, Uppot RN, Samir AE, Gervais DA, Mueller PR. Radiofrequency ablation of hepatic tumours: effect of post-ablation margin on local tumour progression. *Eur Radiol* 2010; **20**: 877–85.
18 Nakazawa T, Kokubu S, Shibuya A *et al.* Radiofrequency ablation of hepatocellular carcinoma: correlation between local tumor progression after ablation and ablative margin. *AJR Am J Roentgenol* 2007; **188**: 480–8.
19 Zytoon AA, Ishii H, Murakami K *et al.* Recurrence-free survival after radiofrequency ablation of hepatocellular carcinoma. A registry report of the impact of risk factors on outcome. *Jpn J Clin Oncol* 2007; **37**: 658–72.
20 Harrison LE, Koneru B, Baramipour P *et al.* Locoregional recurrences are frequent after radiofrequency ablation for hepatocellular carcinoma. *J Am Coll Surg* 2003; **197**: 759–64.
21 Hori T, Nagata K, Hasuike S *et al.* Risk factors for the local recurrence of hepatocellular carcinoma after a single session of percutaneous radiofrequency ablation. *J Gastroenterol* 2003; **38**: 977–81.
22 Shiozawa K, Watanabe M, Wakui N, Ikehara T, Iida K, Sumino Y. Risk factors for the local recurrence of hepatocellular carcinoma after single-session percutaneous radiofrequency ablation with a single electrode insertion. *Mol Med Report* 2009; **2**: 89–95.
23 Fujioka C, Horiguchi J, Ishifuro M *et al.* A feasibility study: evaluation of radiofrequency ablation therapy to hepatocellular carcinoma using image registration of preoperative and postoperative CT. *Acad Radiol* 2006; **13**: 986–94.
24 Niculescu G, Foran DJ, Nosher J. Non-rigid registration of the liver in consecutive CT studies for assessment of tumor response to radiofrequency ablation. *Conf Proc IEEE Eng Med Biol Soc* 2007; **2007**: 856–9.
25 Giesel FL, Mehndiratta A, Locklin J *et al.* Image fusion using CT, MRI and PET for treatment planning, navigation and follow up in percutaneous RFA. *Exp Oncol* 2009; **31**: 106–14.
26 Kim YS, Lee WJ, Rhim H, Lim HK, Choi D, Lee JY. The minimal ablative margin of radiofrequency ablation of hepatocellular carcinoma (>2 and <5 cm) needed to prevent local tumor progression: 3D quantitative assessment using CT image fusion. *AJR Am J Roentgenol* 2010; **195**: 758–65.
27 Kim KW, Lee JM, Klotz E *et al.* Safety margin assessment after radiofrequency ablation of the liver using registration of preprocedure and postprocedure CT images. *AJR Am J Roentgenol* 2011; **196**: 565–72.
28 Okusaka T, Okada S, Ueno H *et al.* Satellite lesions in patients with small hepatocellular carcinoma with reference to clinicopathologic features. *Cancer* 2002; **95**: 1931–7.
29 Carrillo A, Duerk JL, Lewin JS, Wilson DL. Semiautomatic 3-D image registration as applied to interventional MRI liver cancer treatment. *IEEE Trans Med Imaging* 2000; **19**: 175–85.

SCIENTIFIC REPORTS

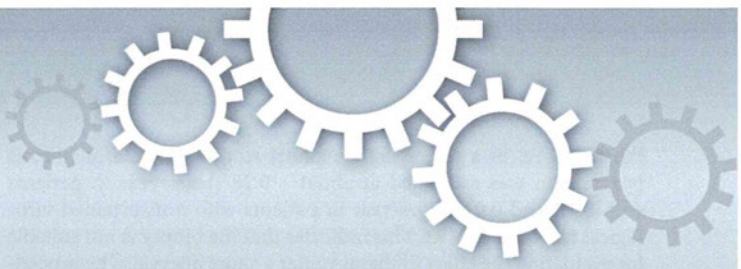

OPEN

SUBJECT AREAS:
GLYCOBIOLOGY
BIOCHEMICAL ASSAYS
ASSAY SYSTEMS
ELISA

Received
3 September 2012

Accepted
27 December 2012

Published
15 January 2013

Correspondence and requests for materials should be addressed to H.N. (h.narimatsu@aist.go.jp)

* These authors contributed equally to this study.

A serum "sweet-doughnut" protein facilitates fibrosis evaluation and therapy assessment in patients with viral hepatitis

Atsushi Kuno[1]*, Yuzuru Ikehara[1]*, Yasuhito Tanaka[2], Kiyoaki Ito[3], Atsushi Matsuda[1], Satoru Sekiya[1], Shuhei Hige[4], Michiie Sakamoto[5], Masayoshi Kage[6], Masashi Mizokami[3] & Hisashi Narimatsu[1]

[1]Research Center for Medical Glycoscience (RCMG), National Institute of Advanced Industrial Science and Technology (AIST), Tsukuba, Japan, [2]Department of Virology & Liver Unit, Nagoya City University Graduate School of Medical Sciences, Nagoya, Japan, [3]The Research Center for Hepatitis and Immunology, National Center for Global Health and Medicine, Ichikawa, Japan, [4]Department of Internal Medicine, Hokkaido University Graduate School of Medicine, Sapporo, Japan, [5]Department of Pathology, School of Medicine, Keio University, Tokyo, Japan, [6]Department of Pathology, Kurume University School of Medicine, Kurume, Japan.

Although liver fibrosis reflects disease severity in chronic hepatitis patients, there has been no simple and accurate system to evaluate the therapeutic effect based on fibrosis. We developed a glycan-based immunoassay, FastLec-Hepa, to fill this unmet need. FastLec-Hepa automatically detects unique fibrosis-related glyco-alteration in serum hyperglycosylated Mac-2 binding protein within 20 min. The serum FastLec-Hepa counts increased with advancing fibrosis and illustrated significant differences in medians between all fibrosis stages. FastLec-Hepa is sufficiently sensitive and quantitative to evaluate the effects of PEG-interferon-α/ribavirin therapy in a short post-therapeutic interval. The obtained fibrosis progression is equivalent to -0.30 stages/year in patients with sustained virological response, and 0.01 stages/year in relapse/nonresponders. Furthermore, long-term follow-up of the severely affected patients found hepatocellular carcinoma developed in patients after therapy whose FastLec-Hepa counts remained above a designated cutoff value. FastLec-Hepa is the only assay currently available for clinically beneficial therapy evaluation through quantitation of disease severity.

The World Health Organization has estimated that the prevalence of chronic infections with hepatitis B virus (HBV) and hepatitis C virus (HCV) is more than 5% of the world population. The high rate of viral transmission worldwide has also resulted in an explosive increase in incidence of liver cirrhosis (LC), because liver fibrosis caused by the persistent infections with HBV and HCV irreversibly progresses in chronic hepatitis (CH) patients without effective treatment. As the incidence of hepatocellular carcinoma (HCC) increases proportionally to the severity of hepatitis and the presence of LC, it is now clear that about 90% of HCC cases originate from infection with HBV or HCV. It is estimated that more than one million patients worldwide die from liver disease related to HBV or HCV infection each year. Immunomodulatory therapy with PEG-interferon-α and ribavirin is the standard treatment for patients with chronic hepatitis C (CHC)[1]. Recent genome-wide association studies have revealed that variation in the host interleukin-28B gene can predict the outcome of therapies for viral clearance[2–4]. Such pharmacokinetic understanding should allow for more precise treatment protocols and follow-up analyses to optimize the opportunity for patients to achieve sustained virological response (SVR)[5,6]. Linear peptidomimetic HCV and NS3/4A serine protease inhibitors such as telaprevir and boceprevir are new drugs that, in combination with PEG-interferon-α and ribavirin, substantially improve the rates of response among patients with HCV genotype 1 infection[1]. Alternatively, suppression of hepatic decompensation in chronic hepatitis B patients with advanced fibrosis and cirrhosis has been evaluated during long-term treatment with antiviral agents, such as adefovir, lamivudine, entecavir, and tenofovir[7]. For example, cumulative entecavir therapy (for at least 3 years) resulted in substantial histological improvement and regression of fibrosis or cirrhosis[8].

The efficacy of therapy is currently evaluated by frequent monitoring of "viral load" or "liver injury"[5]. From the viewpoint of developing preventive strategies for HCC, the risk of HCC development should also be estimated along with them. For this purpose, liver biopsy is generally considered as the gold standard in which fibrosis is subclassified into 5 stages of severity (F0–4). However, this procedure is invasive and shown to cause a high rate of sampling error (about 15% false-negatives for cirrhosis) in patients with diffuse parenchymal liver diseases.

Furthermore, in a retrospective cohort study[9], the rate of fibrosis progression was estimated at about −0.28 stages/year in patients with SVR and 0.02 stages/year in patients with nonsustained virological response (NVR). This indicates that the biopsy is not suitable for evaluating the effect of therapy after a short interval. The procedure has further disadvantages such as inaccuracy, biopsy-related complications, the need for hospitalization, the time involved, and low cost-effectiveness[10]. Therefore, alternative noninvasive assays are desired and should provide a quantifiable readout of fibrosis progression using a method that is accurate, cost-effective and relatively simple.

To date, several methods have been developed[10] including FibroScan, which measures hepatic fibrosis biomechanically as tissue stiffness based on transient elastography. FibroScan has the advantages of being rapid and technically simple; however, its diagnostic success rate is affected by operator skill. Therefore, it has been suggested that FibroScan, in conjunction with assay of serum fibrosis biomarkers, should improve diagnostic accuracy. FibroTest[11] and FibroMeter[12], believed to be the most reliable indices of fibrosis, have been used in the combination assay aiming to eliminate the need for liver biopsy[13,14]. However, FibroTest and FibroMeter do not complement FibroScan in the development of a rapid "on-site diagnosis" system. This is because each requires both extensive and specialized blood analyses (FibroTest requires α2-macroglobulin, apolipoprotein A1, haptoglobin, γ-glutamyltransferase and total bilirubin whereas FibroMeter requires platelet count, prothrombin index, AST, α2-macroglobulin, hyaluronic acid and urea). In addition, both tests require data on age, and also sex for FibroTest.

Glycans are referred to as the face of cells, which reflect their status such as differentiation stage rather than their state of damage, and therefore they can be great markers for chronic disease. In the case of hepatitis, glycans are considered to reflect more specifically the progression of fibrosis than viral load. In the search for a simple and rapid method that is not markedly affected by tissue inflammation and ALT fluctuation, the possibility of glycomic and glycoproteomic techniques has emerged[15,16], and there are reports of some successful examples applicable for use in the clinical laboratories[17–19]. However, the current glycomic techniques require at least 3 hours of sample preparation for analysis and this has markedly reduced the combination use of glycan-based immunoassays with FibroScan. In this report, we describe for the first time, a rapid and simple glycan-based immunoassay, FastLec-Hepa, that can quantify fibrosis as precisely as FibroTest and also readily evaluate the antifibrotic effects of therapy at the clinical site (**Supplementary Fig. 1**). Moreover, we introduce a novel method for rational selection of the "non-fucose binding type" lectins and provide details of how this concept can be adopted for future development of clinically useful glycodiagnostic tools.

Results

Changes in the *N*-glycosylation of M2BP during progression of liver disease. Based on previous reports[20–23], we adopted the serum 90 K/Mac-2 binding protein (M2BP) as a glycoprotein biomarker for liver fibrosis. M2BP is secreted from many cell types, including hepatocytes (http://www.proteinatlas.org/ENSG00000108679), and it has been shown to modulate many processes, particularly those related to cell adhesion. For example, the interaction of M2BP with matrix fibronectin can modulate adhesion and the high expression of M2BP by tumor cells increases the level in the circulation of affected patients. A prominent feature of native human M2BP is its oligomerization to large ring structures[20], resembling a "sugar-powdered doughnut" which is potentially covered with 70–112 *N*-glycans (**Fig. 1a**). To confirm serum M2BP as a valid marker, we performed a pull-down assay with serum (2 μl each) from five individuals in each of the following groups: HCC, LC, CHC or healthy volunteer with normal liver (HV). Although two bands appeared in all HVs and two CHC patients, M2BPs from patients with relatively severe fibrosis, i.e., LC and HCC, migrated as a single band, the mobility of which was similar to that of the lower band for HVs (**Fig. 1b**). Significant increases in band intensity with excessive smearing of the bands were seen for most HCC patients. A subsequent investigation of 125 HCV patients with stage-determined fibrosis showed alteration in the quality and quantity of M2BP during the progression of fibrosis (**Fig. 1c**) and apparent alteration in the amount of each band (**Fig. 1d and e**), as described in the previous investigations[22,23]. M2BP has been shown to have multibranching and sialylated *N*-glycans. Moreover, it has been suggested that extension of polylactosamine on M2BP controls its binding to galectin-3, a major binding partner *in vivo*. Sialylation and extension of polylactosamine affect the charge and size of M2BP and this results in altered electrophoretic migration. Accordingly, we speculate that the size heterogeneity of M2BP seen on electrophoresis is due to such alterations in glycosylation. In fact, the difference in the band migration was eliminated by Sialidase A treatment, and the smearing of the bands in HCC was reduced by treatment with *N*-Glycosidase F (**Supplementary Fig. 2**). These results indicated that the altered quality of M2BP during progression of liver disease was due to changes in *N*-glycosylation.

Selection of the optimal lectin for direct measurement of disease-related M2BP. To construct a reliable assay (see **Supplementary Fig. 3**), we needed to identify a lectin probe that could most readily discriminate the altered *N*-glycans of M2BP and specifically binds to them in serum without pretreatment. For this purpose, we added a subtraction process to our recently described microarray-based selection strategy[16] (**Supplementary Fig. 4**). In brief, we first obtained a typical glycan profile for serum M2BPs by averaging the glycan profiles of M2BPs immunoprecipitated from 125 HCV patient sera by the antibody-overlay lectin microarray[16,18,24] (**step 1**). In this step, we selected 27 lectins binding to M2BP from a 45-lectin array (**Supplementary Fig. 5a**). Most of them bound not only to M2BP (ca. 10 μg/ml in serum), but also to other abundant serum glycoproteins, whereas some suggested rather specific binding to M2BP. We designated them as high-noise lectins or high signal-to-noise (S/N) lectins, respectively (**Fig. 2a**). We then selected the candidate lectins for the assay by subtracting the high-noise lectins from the M2BP-binding lectins (**step 2**), using a glycan profile of whole serum (**Supplementary Fig. 5**)[25]. Comparing the profiles for M2BP and whole serum (**Fig. 2b**), we quickly identified 6 lectins with a high S/N ratio. Interestingly, all lectins identifying fucose modification, which is the most well-known glyco-alteration in liver disease (*Pisum sativum* agglutinin (PSA), *Lens culinaris* agglutinin (LCA), *Aspergillus oryzae* lectin (AOL), and *Aleuria aurantia* lectin (AAL)), were high-noise lectins (**Fig. 2b**). After subtraction, we used both the Mann–Whitney *U* test as a nonparametric test, and receiver-operating characteristic (ROC) analysis, to characterize the diagnostic accuracy of the candidate lectins at each stage of fibrosis: significant fibrosis (F2/F3/F4), severe fibrosis (F3/F4) and cirrhosis (F4) (**step 3**). As a result, we found that the diagnostic score of *Wisteria floribunda* agglutinin (WFA) was superior to the other 5 lectins at every fibrosis stage (**Fig. 2c and Supplementary Fig. 6**).

"Proof-of-concept" experiment for direct quantitation of the serum WFA-binding M2BP by sandwich immunoassay. We quantitatively analyzed the WFA-binding M2BPs (WFA^+-M2BP) in serum. Sera, pretreated as described in the **Methods**, were firstly subjected to affinity capture with 20 μl slurry of WFA-coated agarose gel. The eluted fraction was immunoprecipitated with a capturing antibody against M2BP and the product was analyzed by Western blot. The intensity of the "smearing-band" signal for WFA^+-M2BP gradually increased in proportion to the severity of liver fibrosis (**Supplementary Fig. 7**), as indicated by the red line shown in

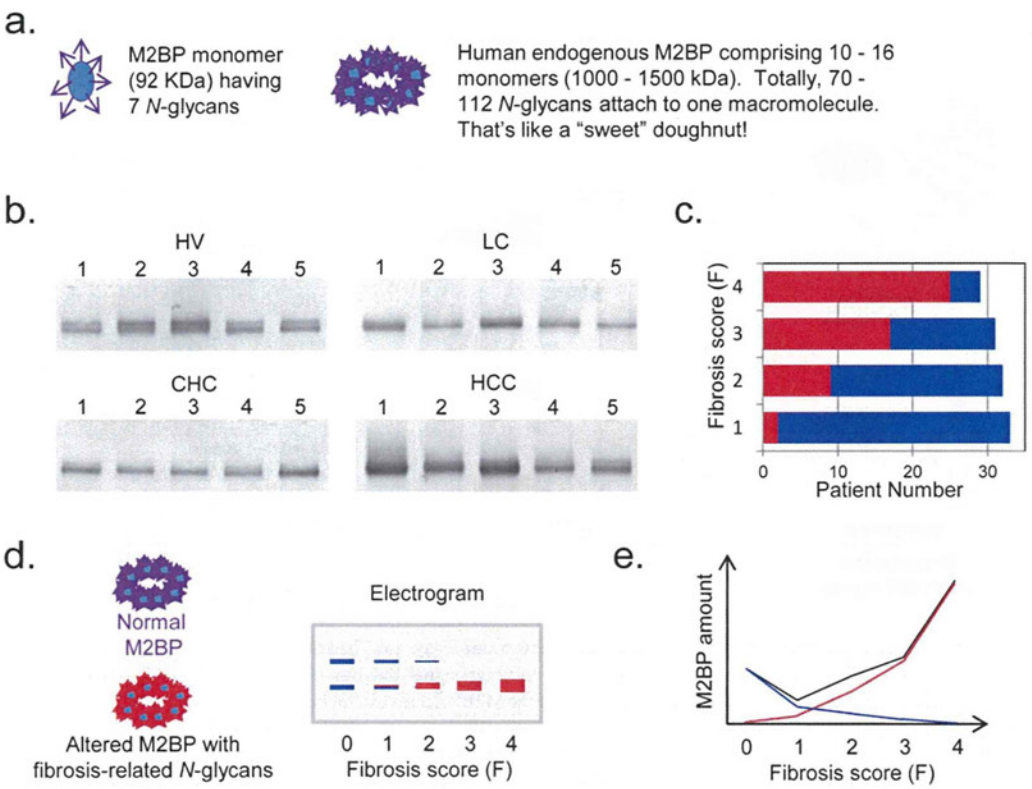

Figure 1 | Changes in the quality and quantity of human serum M2BP with progression of liver fibrosis. (a) The unique shape of human endogenous serum M2BP. The arrowheads and circles represent the *N*-glycan moieties and core protein respectively. (b) Western blot analysis: M2BPs in 2 μl of serum were purified by immunoprecipitation before SDS-PAGE. HV, healthy volunteer; CHC, patient with chronic hepatitis C; LC, HCV-infected patient with liver cirrhosis; and HCC, HCV-infected patient with hepatocellular carcinoma. (c) Number of patients with single (red) or double (blue) band appearance on the blot. The number of bands was determined visually by two independent analysts. The total number of HCV patients who participated in this study was 125 (F0–F1 [$n = 33$], F2 [$n = 32$], F3 [$n = 31$], and F4 [$n = 29$]). (d) Typical changes of serum M2BP band intensities in patients with different fibrosis scores and (e) concentrations based on a previous report on quantitation of serum M2BP by Cheung *et al*[3]. and our present results. The blue bands on the electrogram and blue line on the graph represent M2BPs secreted from normal liver. The red bands and line represent altered M2BP, the concentration of which is suggested to increase with the progression of fibrosis. The black line represents the total concentration of serum M2BP.

Fig. 1e. We next conducted a sandwich immunoassay with WFA and anti-M2BP antibody (see **Supplementary Fig. 3b**). WFA was immobilized on the surface of a 96-well microtiter plate through biotin–streptavidin interaction. We performed the first assay for the WFA-binding activity using recombinant human M2BP (rhM2BP). As a result, a linear regression analysis revealed a linear range of detection from 0.039 to 0.625 μg/ml (**Supplementary Fig. 8a**). Subsequently, we used culture supernatant of a hepatoblastoma cell line HepG2, which expresses WFA^+-M2BP, to illustrate the dose-dependency of the interaction of WFA with M2BP/HepG2. We also showed that heat treatment of the culture supernatant eliminated this binding activity (**Supplementary Fig. 8b**). Finally, we performed a sandwich immunoassay for direct measurement of WFA^+-M2BP in untreated serum samples, and the results correlated well with the quantitative assay using affinity capture and lectin microarray analysis (**Supplementary Fig. 7 and 9**).

FastLec-Hepa: a fully automated sandwich immunoassay for direct quantitation of serum WFA^+-M2BP. We adapted the WFA-antibody immunoassay to the HISCL-2000i bedside clinical chemistry analyzer[18]. We successfully adjusted every reaction condition during the automatic assay by HISCL, which is about a 17-min manipulation. Heat pretreatment of the serum was avoided to ensure both binding avidity and the fast association rate. Repeatability was assessed by performing 10 independent assays of three samples, and the coefficient of variation ranged between 2.1% and 2.5% (data not shown). Sensitivity was determined by triplicate assays of samples generated by 2-fold serial dilution of 50 μg/ml rhM2BP. The linear regression analysis identified a linear range of detection ($R^2 = 1.00$) from 0.025 to 12.5 μg/ml (**Fig. 3a**, a range of 0.025 to 1.6 μg/ml also shown in **Fig. 3b**). The resulting dynamic range was 25-fold that of the manual sandwich immunoassay described above. We next examined whether the HISCL measurements made on serum from HCV patients ($n = 125$) were consistent with lectin microarray analysis, and this comparison resulted in sufficient linearity with coefficient of determination, $R^2 = 0.848$ (**Fig. 3c**). Accordingly, we could perform automatic quantitation of serum WFA^+-M2BP in 180 patients in 1 hour and we have therefore named it FastLec-Hepa.

Validation of FastLec-Hepa. For a validation study, we obtained serum from CH patients at two locations: Nagoya City University Hospital and Hokkaido University Hospital (**Supplementary Fig. 10**). Staging of these patients ($n = 209$) by histological activity index (HAI) was conducted independently by two senior pathologists on ultrasonography-guided liver biopsy samples. F0–F1 was assigned in 82 cases (39.2%), F2 in 52 (24.9%), F3 in 40 (19.1%), and F4 (cirrhosis) in 35 (16.7%). Serum from healthy volunteers (with no history of any hepatitis virus infections) was obtained for analysis from two sites ($n = 48$ from National Institute of Advanced Industrial Science and Technology [AIST]: HV1; $n = 70$ from Nagoya City University: HV2). Their FastLec-Hepa counts

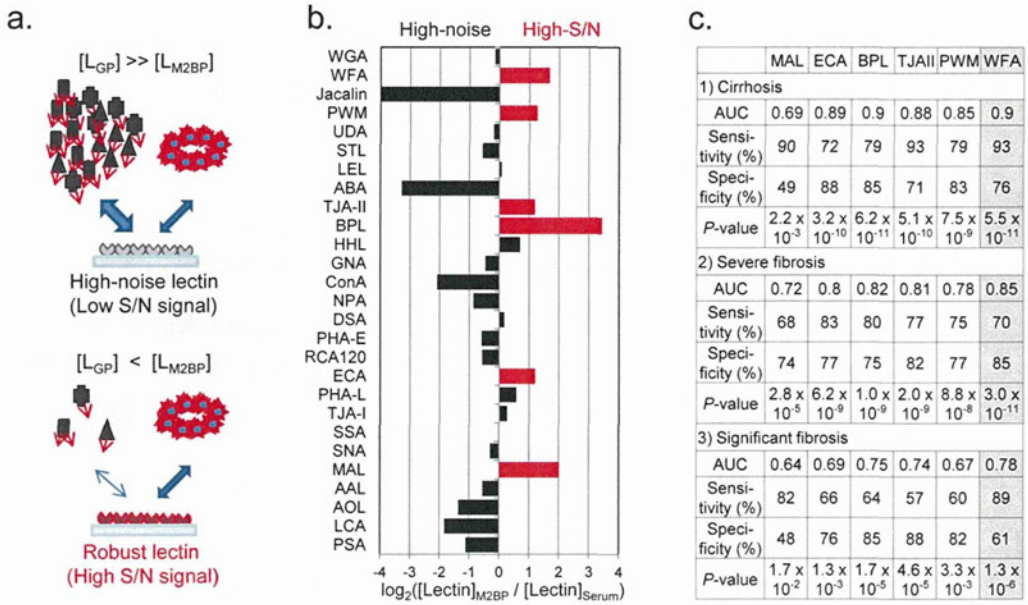

c.

	MAL	ECA	BPL	TJAII	PWM	WFA
1) Cirrhosis						
AUC	0.69	0.89	0.9	0.88	0.85	0.9
Sensitivity (%)	90	72	79	93	79	93
Specificity (%)	49	88	85	71	83	76
P-value	2.2×10^{-3}	3.2×10^{-10}	6.2×10^{-11}	5.1×10^{-10}	7.5×10^{-9}	5.5×10^{-11}
2) Severe fibrosis						
AUC	0.72	0.8	0.82	0.81	0.78	0.85
Sensitivity (%)	68	83	80	77	75	70
Specificity (%)	74	77	75	82	77	85
P-value	2.8×10^{-5}	6.2×10^{-9}	1.0×10^{-9}	2.0×10^{-9}	8.8×10^{-8}	3.0×10^{-11}
3) Significant fibrosis						
AUC	0.64	0.69	0.75	0.74	0.67	0.78
Sensitivity (%)	82	66	64	57	60	89
Specificity (%)	48	76	85	88	82	61
P-value	1.7×10^{-2}	1.3×10^{-3}	1.7×10^{-5}	4.6×10^{-5}	3.3×10^{-3}	1.3×10^{-6}

Figure 2 | Selection of the optimal lectin for the lectin-antibody sandwich immunoassay. (a) The kinetics of lectins binding to serum glycoproteins. The M2BP-binding lectins are divided into two categories: high-noise lectins and high signal-to-noise (S/N) lectins. The high-noise lectins bind to both M2BPs and abundant serum glycoproteins, causing a strong suppression of the M2BP–lectin interaction (see *top panel*). On the other hand, the number of binding targets in serum for the high S/N lectins is negligible, resulting in the specific interaction with the target M2BP (see *lower panel*). (b) Classification of M2BP-binding lectins. The high S/N lectins are those detecting M2BPs with at least twice the signal intensity seen for other serum glycoproteins. The classification strategy is summarized in **Supplementary Fig. 4**. (c) Diagnostic performance of 6 candidate lectins. *P*-values were determined using the nonparametric Mann–Whitney *U* test (Excel 2007, Microsoft).

(**Supplementary Table 1**) are also plotted in a box-whisker diagram in **Supplementary Fig. 11** along with that from a separate group of 1,000 healthy volunteers (HV3). Based on the calibration curve ([FastLec-Hepa counts]/10^6 = 1.027 × [rhM2BP] + 0.006 in **Fig. 3a, b**), the 75th percentiles of HVs of 64,205–107,617 and the 25th percentile of LC of 1,327,596 patients (see also **Supplementary Fig. 11**), we estimate the concentration of WFA$^+$-M2BP to be approximately 0.09 μg/ml in the serum of HV patients and > 1.0 μg/ml in that of LC patients. This means that the linear range shown in **Fig. 3a** is sufficient for accurate quantitation of WFA$^+$-M2BP in all serum samples. The analyses showed a gradual increase with the progression of liver fibrosis, but it did not correlate with the grade of hepatic activity defined by HAI scoring (**Supplementary Fig. 12**).

Next, we made a statistical comparison of FastLec-Hepa with other simple tests for liver fibrosis: the direct fibrosis marker hyaluronic acid (HA), the indirect fibrosis index FIB-4[26] and the glycan-based fibrosis index LecT-Hepa[18,27]. We enrolled 160 patients (F0−F1 = 66, F2 = 41, F3 = 33 and F4 = 20) whose age, platelet count, AST, ALT and HA levels were readily available (**Supplementary Fig. 10** and **Supplementary Tables 1 and 2**). As shown in **Fig. 4a**, the results of all the tests correlated well with the stage of fibrosis ($P < 0.0001$). However, an ROC analysis concluded that FastLec-Hepa detected cirrhosis with the highest diagnostic accuracy (**Fig. 4b** and **Table 1**). Notably, FastLec-Hepa distinguished between F3 and F4 with 90% sensitivity, 85% specificity, and with an AUC of 0.91. These results were superior to LecT-Hepa (sensitivity:

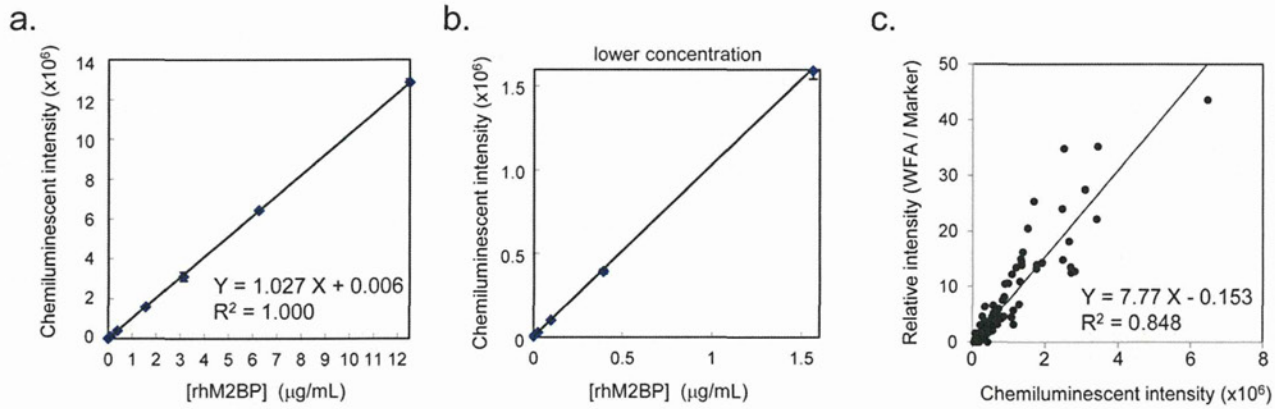

Figure 3 | Description of FastLec-Hepa, a fully automated WFA and anti-M2BP antibody sandwich immunoassay. (a) Standard curve for quantitation of WFA-binding rhM2BP. Plots for the lower concentration of rhM2BP are alternatively highlighted in (b). (c) Scatterplot comparison of WFA$^+$-M2BP data obtained from 125 different serum samples by both HISCL and a manual lectin microarray assay. The best-fit linear comparison with its correlation coefficient was calculated in Excel 2007 (Microsoft).

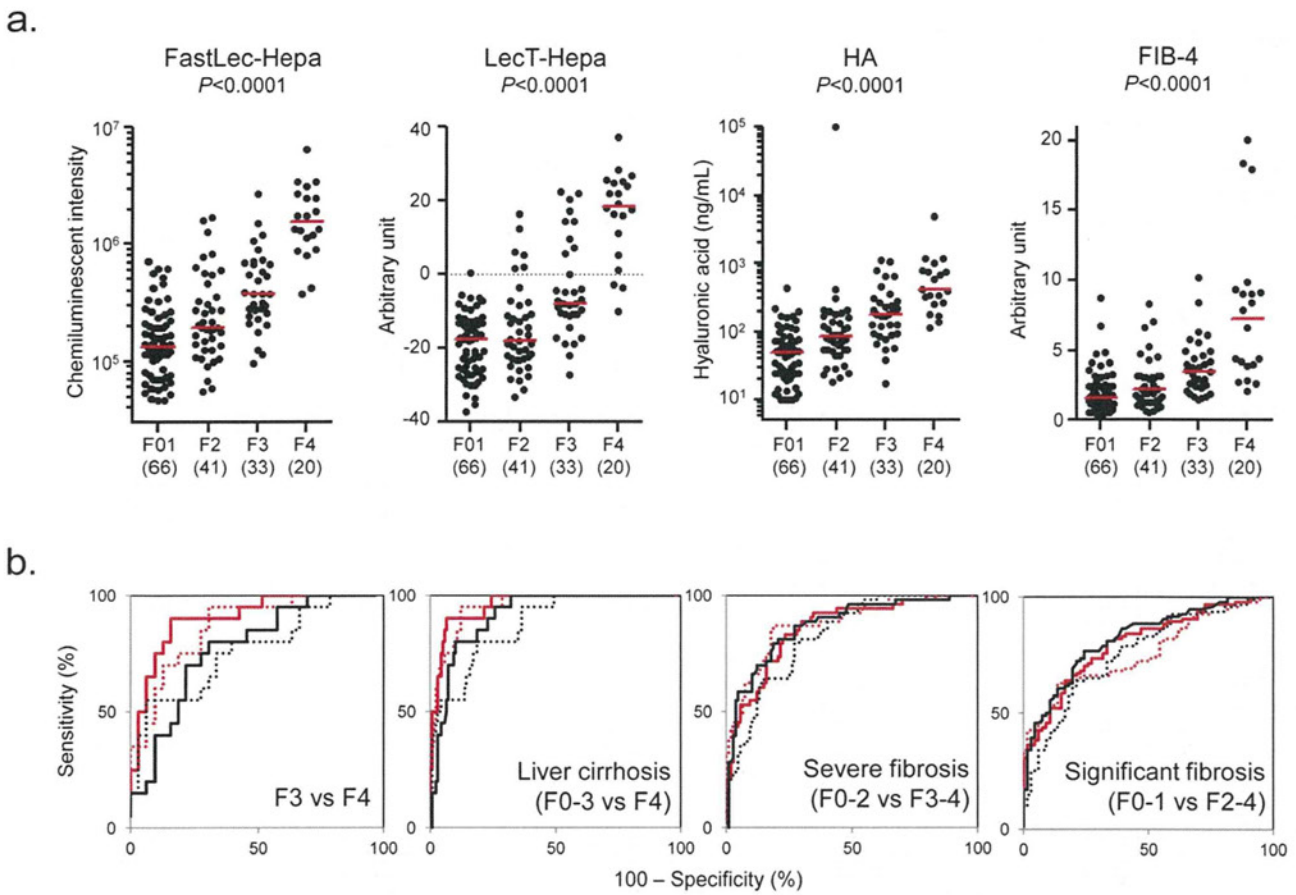

Figure 4 | Comparison of diagnostic performance of FastLec-Hepa, LecT-Hepa, HA, and FIB-4. (a) Scatterplots of the data obtained with FastLec-Hepa, LecT-Hepa, HA, and FIB-4 against the fibrosis score. Red horizontal lines represent the median. Correlation of the data with the progression of fibrosis was evaluated as significant differences in the medians relative to the fibrosis scores ($P < 0.0001$) by a nonparametric method, the Kruskal–Wallis one-way ANOVA. (b) Area under the receiver-operating characteristic (AUC-ROCs) curves of FastLec-Hepa, LecT-Hepa, HA, and FIB-4 for liver cirrhosis (F3 vs F4 or F0–3 vs F4), severe fibrosis (F0–2 vs F3–4), and significant fibrosis (F0–1 vs F2–4). FastLec-Hepa, LecT-Hepa, HA, and FIB-4 are indicated by a red solid line, red dotted line, black solid line, and black dotted line, respectively.

95%, specificity: 70%, and AUC: 0.87), FIB-4 (sensitivity: 55%, specificity: 94%, and AUC: 0.76), and HA (sensitivity: 80%, specificity: 70%, and AUC: 0.78).

Clinical utility of FastLec-Hepa: quantitative monitoring of antiviral therapy. To assess clinical utility, we examined two types of trials—short-interval evaluation and long-term follow-up—both of which are essential for following the patients receiving PEG-interferon-α and ribavirin therapy. For the first trial, we enrolled 41 patients with CHC who had previously undergone 48 weeks of therapy at Hokkaido University Hospital. According to the definition described in the **Methods**, 26 and 15 of them were judged as SVR and NVR/relapse (non-SVR), respectively. For each patient, we performed FastLec-Hepa on serum samples, which were collected just before treatment (Pre) and within a short period (12–22 weeks) after treatment (Post) (**Fig. 5a**). We found a marked decrease from Pre to Post counts ($P = 0.0061$) in SVR patients, but no apparent change for non-SVR patients ($P = 0.9780$) (**Fig. 5b**). Specifically, a median percent decrease of 31% was found for SVR patients (median Pre-count of 161,053 and median Post-count of 110,739), while the level for non-SVR patients was essentially constant. These results show that the assay can evaluate the effect of therapy within a short period after treatment. This is an important advance, because the ALT levels of non-SVR, as well as SVR, are mostly decreased into the range of 10–64 IU/ml during this period (**Fig. 5c**)[5]. In fact, changes in the FastLec-Hepa counts did not correlate with those in the ALT counts (**Supplementary Fig. 13**), thereby invalidating ALT-dependent fibrosis assays, including FIB-4 (**Fig. 5d**).

In support of our finding that the FastLec-Hepa counts correlate excellently with the stage of fibrosis, we found a strong correlation between the histopathological scores and the median of the $\log_{10}$[FastLec-Hepa] counts (**Fig. 5e**). These correlations were approximated to two linear equations: $y = 0.23x + 4.9$ for F0 to F3, and $y = 0.58x + 3.8$ for F3 to F4 histology. This means that FastLec-Hepa can reliably reproduce the assessment of therapeutic effects, which were previously drawn from histopathological scoring[9]. Indeed, the median changes in fibrosis obtained by FastLec-Hepa analysis were about −0.295 stages/year for SVR and 0.010 stages/year for non-SVR (**Fig. 5f**). These data were consistent with the rate of fibrosis progression and regression determined by Shiratori *et al*[9].

For the second trial, we enrolled 6 HCV patients (SVR = 3 and non-SVR = 3) with advanced fibrosis who completed 48 weeks of therapy at Nagoya City University Hospital. Sera were collected before therapy and at 0, 1, 3, and 5 years after the end of therapy (see **Fig. 5g**). FastLec-Hepa counts in SVR patients gradually decreased and reached below the median of F0 patients within 3 years. However, those in non-SVR patients remained above the median for F3 patients during the follow-up period (**Fig. 5h**).

Table 1 | Diagnostic performance of fibrosis markers

n = 160	FIB-4	HA	LecT-Hepa	FastLec-Hepa
a) Significant fibrosis (F0–1 vs F2–4)				
AUC	0.76	0.82	0.76	0.79
(95% CI)	(0.68–0.83)	(0.76–0.89)	(0.69–0.83)	(0.72–0.86)
Diagnostic sensitivity (%)	64	77	63	81
Diagnostic specificity (%)	79	76	86	67
Youden's index (%)	43	52	49	48
b) Severe fibrosis (F0–2 vs F3–4)				
AUC	0.83	0.87	0.88	0.84
(95% CI)	(0.76–0.89)	(0.81–0.93)	(0.82–0.93)	(0.77–0.91)
Diagnostic sensitivity (%)	81	81	87	83
Diagnostic specificity (%)	71	79	81	77
Youden's index (%)	52	61	68	60
c) Liver cirrhosis (F0–3 vs F4)				
AUC	0.88	0.91	0.95	0.96
(95% CI)	(0.80–0.95)	(0.86–0.96)	(0.92–0.99)	(0.93–0.99)
Diagnostic sensitivity (%)	80	80	95	90
Diagnostic specificity (%)	81	90	88	94
Youden's index (%)	61	70	83	84
d) Liver cirrhosis (F3 vs F4)				
AUC	0.76	0.78	0.87	0.91
(95% CI)	(0.63–0.90)	(0.65–0.90)	(0.77–0.97)	(0.82–0.99)
Diagnostic sensitivity (%)	55	80	95	90
Diagnostic specificity (%)	94	70	70	85
Youden's index (%)	49	50	65	75

Interestingly, HCC had developed in two non-SVR patients whose FastLec-Hepa counts remained above the median of F4 patients throughout. Other fibrosis indices, such as FIB-4 and biochemical parameters (ALT and AST), did not distinguish between SVR and non-SVR or appear to predict this occurrence (**Fig. 5i-k**).

Discussion

We have described the development and use of a fully automated, glycan-based immunoassay termed FastLec-Hepa, for the evaluation of liver fibrosis. A high degree of reliability in the quantitative aspects of this method should establish it as a clinically significant test,

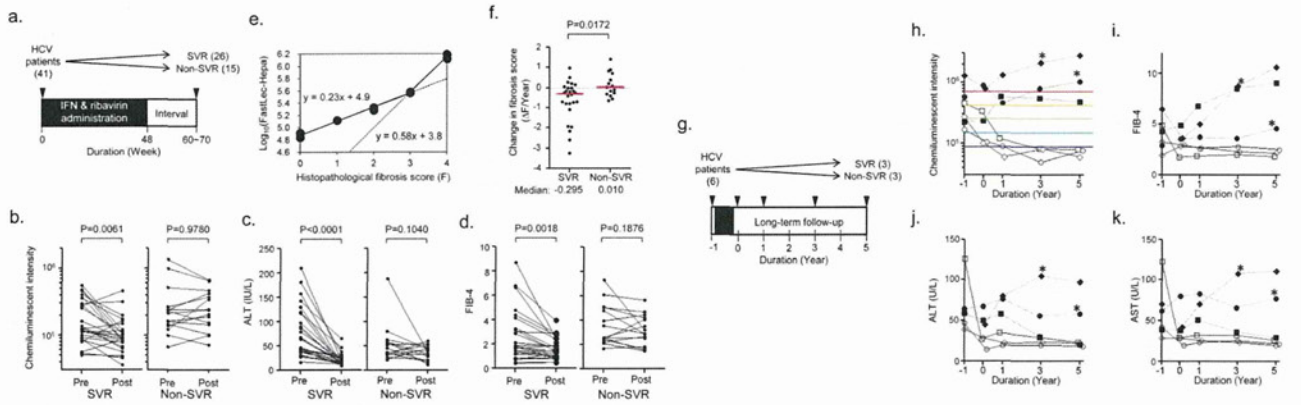

Figure 5 | Evaluation of the curative effect of interferon therapy by FastLec-Hepa. (a) Validation of FastLec-Hepa in short-interval evaluation. The numbers in parentheses represent the number of patients participated in this experiment. Arrowheads indicate the timing of blood collection. At week 0, blood was collected immediately before the treatment. Black box indicates the period of PEG-interferon-α and ribavirin therapy. Changes in the FastLec-Hepa counts (b), ALT (c), and the FIB-4 index (d) in patients with sustained virologic response (SVR) and relapse/nonresponders (non-SVR) during interferon therapy. The *P*-value was determined by a nonparametric method, the Wilcoxon matched pairs signed-rank test. (e) Dot-plot representation of the histopathological fibrosis score and the medians of FastLec-Hepa counts. Best-fit linear curves were calculated in Excel 2007 (Microsoft) allowing conversion of the FastLec-Hepa counts into fibrosis score. (f) Yearly changes in the converted fibrosis score. Changes for patients with SVR and non-SVR are indicated in the dot plots. Red horizontal lines represent the median. The *P*-value was determined by the Mann–Whitney *U* test. (g) Validation of FastLec-Hepa in long-term follow-up. The numbers in parentheses represent the number of patients participated in this experiment. Arrowheads indicate the timing of blood collection. At year -1 and 0, the blood was collected immediately before and after the treatment, respectively. Black box indicates the period of PEG-interferon-α and ribavirin therapy. Yearly changes of FastLec-Hepa counts (h), FIB-4 index (i), ALT (j), and AST (k) in individual patients after therapy. The five colored lines in (h) represent the median values obtained for each fibrosis stage (red, F4; orange, F3; green, F2; cyan, F1; blue, F0). Closed and opened symbols indicate the data obtained from non-SVR and SVR patients, respectively. * indicates the period when the development of HCC was found.

particularly for revealing and managing patients at a high risk of progression to liver complications such as HCC and related life-threatening events. The most striking advantage of FastLec-Hepa is not only its simplicity but also its capacity to provide fibrosis read-outs that are not influenced by fluctuations in the ALT value or inflammation, both of which can cause falsely high estimates in most of the other fibrosis tests available[10]. In fact, our study has illustrated robust capacity of FastLec-Hepa to evaluate the effects of antiviral therapy and subsequent disease progression in both the short and long term.

Many retrospective and prospective studies have demonstrated that achieving SVR through the PEG-interferon-α/ribavirin treatment significantly reduces liver-related morbidity and mortality (i.e., hepatic decompensation, HCC, and liver-related death)[28–30]. As this combination therapy is effective in only about 50% of patients with HCV genotype 1, new agents[1] and targets[31] for antiviral treatments of HCV have been developed to achieve SVR more effectively after the therapy. Long-term follow-ups often show that the risk of disease progression is significantly high in patients with non-SVR after PEG-interferon-α/ribavirin treatment. Furthermore, the development of HCC in patients with SVR remains at a significant cumulative rate (2%)[28,30,32,33]. For these reasons, a new data-mining model using individual factors (age, platelet count, serum albumin and AST) was developed recently to identify patients at a high risk of HCC development[34]. This is, however, a statistical procedure for estimating the chance of disease progression, and there is not a direct evaluation of fibrosis. In the present report, we performed a long-term retrospective study with serially collected sera from SVR and non-SVR patients, in which we showed the potential use of FastLec-Hepa for improved prognostic accuracy. Indeed, recent advances in the development of antifibrotic agents lead us to expect the therapeutic elimination of health risks associated with HCC and decompensation[35]. Moreover, we expect that FastLec-Hepa will be proved for its usefulness in rapid evaluation of progression and regression of fibrosis in clinical trials of newly developed antifibrotic agents. Hence, FastLec-Hepa should be very useful for fibrosis stage screening and evaluation of disease progression in untreated individuals or patients under or after treatment, as well as evaluation of the most recently developed drugs.

It is important to note that FastLec-Hepa has many merits, including speed (possibly 1,000 assays per day) and full automation for measurement of a serological glycobiomarker: these attributes will enable retrospective studies with valuable serum specimens that have been collected previously. In addition, our recently developed calibrator for FastLec-Hepa will improve traceability and enable simultaneous assay and data storage in multiple diagnostic facilities. The data obtained with diluted serum samples demonstrated a high level of assay reproducibility and a very favorable linear detection range (**Supplementary Fig. 14**). Furthermore, we found an excellent agreement between assay values for serum and plasma prepared simultaneously from the same patient. Presently, we have about 10,000 sera and plasma available with detailed clinical notes collected in more than 10 facilities in Japan, and a series of retrospective studies is under way. We will shortly conclude licensing of our system for clinical implementation, based largely on the trials of the present study. In contrast to this, the majority of recent noninvasive techniques are currently shifting to physical measurements such as FibroScan, acoustic radiation force impulse[36] and real-time strain elastography[37]. Any on-site assay of large numbers of blood samples should provide a diagnostic value comparable to that of FibroTest, and a direct comparison in the same patient group will be necessary to evaluate this. We note here that according to a recent statistical validation method[38], predicted AUC of the diagnostic value of FibroTest for detection of advanced fibrosis in our sample set (DANA score = 1.81) was approximately 0.77, which was comparable to the AUC of FastLec-Hepa we obtained (0.79).

FastLec-Hepa has adopted a new paradigm for clinical diagnosis, "glyco-diagnosis", which is based on the quantity and quality of protein glycosylation patterns that well indicate disease progression. To detect such changes in glycosylation by conventional methods (e.g., mass spectrometry, liquid chromatography, or capillary electrophoresis), it is absolutely necessary to liberate the glycans of interest from their protein linkages[15,17,39]. It is possible to employ an alternative technology, which is based on a lectin–antibody sandwich immunodetection system for intact glycoproteins bearing disease-specific glyco-alterations. Such assays have been used to detect changes in fucosylation of *N*-linked glycans, which are associated with liver disease. However, in the present study, fucose-binding lectins were classified as "high noise" (**Fig. 2b**), and thus an enrichment of the target protein was the essential process in the assay. Lectin-overlay detection is performed typically after on-plate enrichment of the target glycoproteins by an immobilized antibody. In such cases, detection relies on a low avidity (high dissociation rate) between the captured glycoprotein and the overlaid lectin probe (see *right* of **Supplementary Fig. 3b**). These kinetic considerations essentially eliminate the use of an automated bedside clinical chemistry analyzer. Even though a fucose-binding lectin was immobilized on the beads (see *left* of **Supplementary Fig. 3b**), it still remains a problem for reliable quantitation by autoanalyzer. Our previous system LecT-Hepa[16,18,19,26], which detects the level of fucosylated α1-acid glycoprotein, requires enrichment of the protein prior to the assay.

In the present study, we have developed a strategy to overcome these problems in glyco-diagnosis associated with clinical implementation, and realized a rapid "on-site diagnosis" system (17 min, within the minimum time required for single assay by HISCL), based on analysis of a glycomarker (**Supplementary Fig. 1**). The strategy for selecting the most robust lectin led us to WFA, and away from the use of fucose-binding lectins, for the direct measurement system (**Fig. 2**). The diagnostic utility of M2BP, a protein resembling "sweet-doughnut"[20], brought a favorable density and orientation of the disease-related glycan on the homomultimer. These characteristic structures resulted in a major increase in the avidity of M2BP for the plated WFA. The resulting glycan–lectin interaction, which is remarkably strong and specific, made it possible to develop the rapid and highly sensitive assay (see *left* of **Supplementary Fig. 3b**). We believe that this unique strategy will revolutionize the use of glyco-diagnosis in clinical medicine and potentially provide a framework for the development of a new generation of biomarker assays.

Methods

Patient samples, biochemical parameters and indices. Patients with chronic hepatitis were enrolled at Nagoya City University Hospital and Hokkaido University Hospital. Healthy volunteers as the controls were randomly selected in Nagoya City University Hospital (70 individuals) and AIST (48 individuals). The institutional ethics committees at Nagoya City University Hospital, Hokkaido University Hospital, and AIST approved this study, and informed consent for the use of their clinical specimens was obtained from all participants before the collection. In addition, we used 1,000 serum samples from virus-negative Caucasians as the normal population, which were purchased from Complex Antibodies Inc. (Fort Lauderdale, FL) and collected under IRB-approved collection protocols. Fibrosis was graded in the patients according to the histological activity index (HAI) using biopsy or surgical specimens. Biopsy specimens were classified as follows: F0, no fibrosis; F1, portal fibrosis without septa; F2, few septa; F3, numerous septa without cirrhosis; and F4, cirrhosis. The three diagnostic targets in this study were defined as significant fibrosis: F2+F3+F4; severe fibrosis: F3+F4; and cirrhosis: F4. Hepatic inflammation was also assessed according to the HAI, as follows: A0, no activity; A1, mild activity; A2, moderate activity; and A3, severe activity. Cirrhosis was confirmed by ultrasonography (coarse liver architecture, nodular liver surface, and blunt liver edges), evidence of hypersplenism (splenomegaly on ultrasonography) and/or a platelet count of $< 100{,}000/mm^3$. Virological responses during PEG-interferon-α and ribavirin therapy were defined as follows[5]: SVR, absence of HCV RNA from serum 24 weeks following discontinuation of therapy; nonresponder, failure to clear HCV RNA from serum after 24 weeks of therapy; relapse, reappearance of HCV RNA in serum after therapy was discontinued. For all patients, age and sex were recorded and serum levels of the following were analyzed: aspartate aminotransferase (AST), alanine aminotransferase (ALT), γ-glutamyltransferase (GGT), total bilirubin,

albumin, cholinesterase, total cholesterol, platelet count (PLT), hyaluronic acid (HA). The FIB-4 index was calculated as follows: [age (years) × AST (U/L)]/[platelets (10^9/L) × ALT (U/L)$^{1/2}$][26]. Fibrosis-specific glyco-alteration of α1-acid glycoprotein was determined by lectin–antibody sandwich immunoassays with a combination of three lectins (*Datura stramonium* agglutinin (DSA), *Maackia amurensis* leukoagglutinin (MAL), and *Aspergillus oryzae* lectin (AOL))[16]. All assays used an automated chemiluminescence enzyme immunoassay system (HISCL-2000i; Sysmex Co., Kobe, Japan)[18].

Enrichment of M2BP from serum. An automated protein purification system (ED-01; GP BioSciences Ltd., Yokohama, Japan) was used to immunoprecipitate M2BP from serum specimens. In brief, sera (2 μl) were diluted 10-fold with PBS/0.2%(w/v) SDS, heated at 95°C for 20 min, mixed with 10 μl of Triton X-100 in TBS (TBSTx) and injected into a 96-well SUMILON microtiter plate (Sumitomo Bakelite Co., Ltd., Tokyo, Japan). The plate and working reagents, including biotinylated anti-M2BP antibody (10 ng/μl), streptavidin-coated magnetic beads, washing buffer (1% TBSTx) and elution buffer (TBS containing 0.2% SDS), were loaded into the system. This generated 110 μl of purified M2BPs per serum sample (96 samples in 3.5 h).

Western blot analysis. Anti-human M2BP polyclonal antibody was purchased from R&D Systems, Inc. (Minneapolis, MN) and biotinylated with Biotin Labeling Kit – NH_2 (Dojindo Laboratories, Kumamoto, Japan). Purified serum M2BPs were electrophoresed under reducing conditions on 5–20% polyacrylamide gels (DRC, Tokyo, Japan) and transferred to PVDF membranes. After treatment with Block Ace® (DS Pharma Biomedical Co., Ltd., Osaka, Japan), the membranes were incubated with biotinylated anti-M2BP polyclonal antibody, and then with alkaline phosphatase-conjugated streptavidin (1/5000 diluted with TBST; ProZyme, Inc., San Leandro, CA). The membranes were incubated with Western Blue stabilized substrate for alkaline phosphatase (Promega, Madison, WI).

Lectin microarray analysis. Enriched M2BPs were analyzed with an antibody-overlay lectin microarray[24]. Purified protein (14 μl) was diluted to 60 μl with PBS containing 1%(v/v) Triton X-100 (PBSTx); this was applied to a LecChip™ (GP BioSciences Ltd.), which included three spots of 45 lectins in each of seven reaction wells. After incubation for 12 h at 20°C, 2 μl of human serum IgG (10 mg/ml) was added to the reaction solution on each chip and incubated for 30 min. The reaction solution was then discarded, and the chip was washed three times with PBSTx. Subsequently, 60 μl (200 ng) of biotinylated anti-human M2BP in PBSTx was applied to the chip, and incubated for 1 h. After three washes with PBSTx, 60 μl (400 ng) of a Cy3-labeled streptavidin (GE Healthcare, Buckinghamshire, UK) solution in PBSTx was added and incubated for 30 min. The chip was rinsed with PBSTx, scanned with an evanescent-field fluorescence scanner (GlycoStation™ Reader1200; GP BioSciences Ltd.) and analyzed with the Array Pro Analyzer software package, version 4.5 (Media Cybernetics, Inc., Bethesda, MD). The chip was scanned with the gain set to register a maximum net intensity < 40,000 for the most intense spots. The net intensity value for each spot was calculated by subtracting the background value from the signal intensity value. The relative intensity of lectin-positive samples was determined from the ratio of their fluorescence to the fluorescence of the internal-standard lectin, DSA.

Quantitation of *Wisteria floribunda* agglutinin (WFA)-binding M2BP. Serum was pretreated as described above under enrichment of M2BP from serum. Pretreated samples (50 μl) were diluted with an equal volume of starting buffer (0.1%(w/v) SDS in PBSTx), added to the WFA-coated agarose in a microtube (20 μl slurry; Vector Lab., Burlingame, UK), and incubated at 4°C for 5 h with gentle shaking. After centrifugation of the reaction solution at 2000 × *g* for 10 min, the supernatant was removed to a new microtube. The precipitate was suspended in 50 μl of the starting buffer, recentrifuged and this second supernatant combined with the first (designated as path-through fraction T). The precipitate was then washed with 200 μl of the starting buffer and the bound glycoproteins were eluted with 60 μl of 200 mM galactosamine/0.02%(w/v) SDS in PBS (designated as elution fraction E). M2BP was immunoprecipitated from fractions T and E and examined by electrophoresis under reducing conditions on 5–20% gradient SDS–polyacrylamide gels.

WFA-antibody sandwich ELISA. Flat-bottomed 96-well streptavidin-precoated microtiter plates (Nunc, Int., Tokyo, Japan) were treated with biotinylated WFA (Vector, 250 ng/well) for 1 h at room temperature. The plates were incubated with the diluted serum samples (50 μl) in PBS containing 0.1%(v/v) Tween20 (PBS-t) for 2 h at room temperature and then with 50 ng/well of the anti-human M2BP polyclonal antibody, in PBS-t for 2 h at room temperature. The plates were washed extensively and then incubated with 50 μl of horseradish peroxidase (HRP)-conjugated anti-mouse IgG (Jackson ImmunoResearch Laboratories Inc., Philadelphia, PA) at 1:10,000 in PBS-t for 1 h at room temperature. The substrate 3,3′,5,5′-tetramethylbenzidine (Thermo Fisher Scientific, Fremont, CA) solution (100 μl) was added to each well. The enzyme reaction was stopped by adding 100 μl of 1 M sulfuric acid, and the optical density measured at 450 nm.

WFA-antibody sandwich immunoassay by HISCL. The fibrosis-specific form of glycosylated M2BP was measured based on a sandwich immunoassay approach. Glycosylated M2BP was captured by WFA immobilized on magnetic beads, and the bound product was assayed with an anti-human M2BP monoclonal antibody linked to alkaline phosphatase (ALP-αM2BP). Two reagent packs (M2BP-WFA detection pack and a chemiluminescence substrate pack) were loaded in the HISCL. The detection pack comprised three reagents: a reaction buffer solution (R1), a WFA-coated magnetic beads solution (R2) and an ALP-αM2BP solution (R3). The chemiluminescence substrate reagent pack contained a CDP-Star substrate solution (R4) and a stopping solution (R5). Typically, serum (10 μl) was diluted to 60 μl with R1 and then mixed with R2 (30 μl). After the binding reaction, R3 (100 μl) was added to the reaction solution. The resultant conjugates were magnetically separated from unbound components, and mixed well with R4 (50 μl) and R5 (100 μl) before reading of the fluorescence. The chemiluminescent intensity was acquired within a period of 17 min in the operation described above. The reaction chamber was kept at 42°C throughout.

Statistics. Statistical analyses and graph preparation used Dr. SPSS II Windows software (SPSS Co., Tokyo, Japan), GraphPad Prism 5.0 (GraphPad Software Inc., La Jolla, CA), and Windows Excel 2007. This facilitated selection of the optimal lectin for analysis of fibrosis and a comparison of the diagnostic value of other serological fibrosis markers and indices. Because the data distribution for each parameter was non-Gaussian, the *P*-values were determined by nonparametric tests, such as the Mann–Whitney *U* test and Wilcoxon signed-rank test. Correlations with liver fibrosis were estimated as the significance of differences among the staging groups (F0–1, F2, F3, and F4) determined by Kruskal–Wallis nonparametric one-way analysis of variance. To assess classification efficiencies for detecting significant fibrosis, severe fibrosis and cirrhosis, the receiver-operating characteristic (ROC) curve analysis was also carried out to determine the area under the curve (AUC) values. Cutoff values obtained from Youden's index were used to classify patients. Diagnostic accuracy was expressed in terms of specificity, sensitivity and AUC.

1. "Nature Outlook Hepatitis C" edited by Brody, H. *et al. Nature* **474**, S1–S21 (2011).
2. Ge, D. *et al.* Genetic variation in IL28B predicts hepatitis C treatment-induced viral clearance. *Nature* **461**, 399–401 (2009).
3. Suppiah, V. *et al.* IL28B is associated with response to chronic hepatitis C interferon-alpha and ribavirin therapy. *Nat. Genet.* **41**, 1100–1104 (2009).
4. Tanaka, Y. *et al.* Genome-wide association of IL28B with response to pegylated interferon-alpha and ribavirin therapy for chronic hepatitis C. *Nat. Genet.* **41**, 1105–1109 (2009).
5. Ghany, M. G., Strader, D. B., Thomas, D. L. & Seeff, L. B. Diagnosis, management, and treatment of hepatitis C: an update. *Hepatology* **49**, 1335–1374 (2009).
6. Afdhal, N. H. *et al.* hepatitis C pharmacogenetics: state of the art in 2010. *Hepatology* **53**, 336–345 (2011).
7. Peng, C. Y., Chien R. N. & Liaw, Y. N. Hepatitis B virus-related decompensated liver cirrhosis: benefits of antiviral therapy. *J. Hepatol.* **57**, 442–450 (2012).
8. Chang, T. T. *et al.* Long-term entecavir therapy results in the reversal of fibrosis/cirrhosis and continued histological improvement in patients with chronic hepatitis B. *Hepatology* **52**, 886–893 (2010).
9. Shiratori, Y. *et al.* Histologic improvement of fibrosis in patients with hepatitis C who have sustained response to interferon therapy. *Ann. Intern. Med.* **132**, 517–524 (2000).
10. Castera, L. Non-invasive assessment of liver fibrosis in chronic hepatitis C. *Hepatol. Int.* **5**, 625–634 (2011).
11. Imbert-Bismut, F. *et al.* Biochemical markers of liver fibrosis in patients with hepatitis C virus infection: a prospective study. *Lancet* **357**, 1069–1075 (2001).
12. Calès, P. *et al.* A novel panel of blood markers to assess the degree of liver fibrosis. *Hepatology* **42**, 1373–1381 (2005).
13. Castera, L. *et al.* Prospective comparison of two algorithms combining non-invasive methods for staging liver fibrosis. *J. Hepatol.* **52**, 191–198 (2010).
14. Boursier, J. *et al.* Comparison of eight diagnostic algorithm for liver fibrosis in hepatitis C: new algorithms are more precise and entirely noninvasive. *Hepatology* **55**, 58–67 (2012).
15. Callewaert, N. *et al.* Noninvasive diagnosis of liver cirrhosis using DNA sequencer-based total serum protein glycomics. *Nat. Med.* **10**, 429–434 (2004).
16. Kuno, A. *et al.* Multilectin assay for detecting fibrosis-specific glyco-alteration by means of lectin microarray. *Clin. Chem.* **57**, 48–56 (2011).
17. Vanderschaeghe, D. *et al.* High-throughput profiling of the serum N-glycome on capillary electrophoresis microfluidics systems: toward clinical implementation of GlycoHepatoTest. *Anal. Chem.* **82**, 7408–7415 (2010).
18. Kuno, A. *et al.* LecT-Hepa: A triplex lectin-antibody sandwich immunoassay for estimating the progression dynamics of liver fibrosis assisted by a bedside clinical chemistry analyzer and an automated pretreatment machine. *Clin. Chim. Acta* **412**, 1767–1772 (2011).
19. Du, D. *et al.* Comparison of LecT-Hepa and FibroScan for assessment of liver fibrosis in hepatitis B virus infected patients with different ALT levels. *Clin. Chim. Acta* **413**, 1796–1799 (2012).
20. Sasaki, T., Brakebusch, C., Engel, J. & Timpl, R. Mac-2 binding protein is a cell-adhesive protein of the extracellular matrix which self-assembles into ring-like structures and binds beta1 integrins, collagens and fibronectin. *EMBO J.* **17**, 1606–1613 (1998).
21. Iacovazzi, P. A. *et al.* Serum 90K/MAC-2BP glycoprotein in patients with liver cirrhosis and hepatocellular carcinoma: a comparison with alpha-fetoprotein. *Clin. Chem. Lab. Med.* **39**, 961–965 (2001).